University of Reading

School of Mathematics, Meteorology & Physics

THE POINT SOURCE METHOD IN INVERSE ACOUSTIC SCATTERING

by

Mark Webber

September 1st, 2004

This dissertation is submitted to the Department of Mathematics in partial fulfilment of the requirements for the degree of Master of Science

Abstract

We pose the direct and inverse problems in acoustic scattering, both informally and mathematically, and detail a method for computing the solution to the direct problem. We present the point source method of R. Potthast as a way to solve the inverse problem for a sound-soft scatterer, which is shown to be ill-posed. A thorough account of the method is given, as well as an error analysis, before detailing a method for its successful implementation in two dimensions. We briefly describe the technique of Tikhonov regularisation as a means of finding solutions to ill-posed problems, and its implementation in the solution of the inverse problem. We include numerical results for the solution of both the direct and inverse problems in two dimensions.

Declaration

I confirm that this is my own work, and the use of all material from other sources has been properly and fully acknowledged.

Mark Webber

Acknowledgements

I would like to acknowledge the help of Professor Simon Chandler-Wilde, for all his assistance in the completion of this dissertation. I would also like to mention the support and encouragement of everyone in the department over the past year, especially those on the MSc course, and Dr Peter Sweby and Professor Michael Baines.

Finally, I would like to recognise the EPSRC for its financial assistance.

Contents

List of Figures

Chapter 1

Introduction

In the modern world there are many examples of wave scattering problems. In designing a music hall, the architect will team up with engineers to model how acoustic waves are scattered by the building's architecture. To check on the progress of her unborn child, a pregnant mother undergoes an 'ultra sound', a procedure whereby high frequency acoustic waves are directed into the womb, and an image of the baby is reconstructed by analysing the field of the scattered waves. Both of these are practical applications of scattering theory, and illustrate the two categories that scattering problems fall into: the *direct scattering problem* and the *inverse scattering problem*.

We model a wave by its *field*, which can be either a scalar or vector valued complex function of time and space. The direct scattering problem is where we use knowledge about the *scatterer* (the object we wish to scatter waves from) and the field due to the incident waves, to determine the field corresponding to the scattered waves, and therefore the *total field* (which is the sum of these two fields). The inverse problem is where we use knowledge of the total field to determine properties of the scatterer (for instance, its shape and location). However, we shall see that we must have some *a priori* information about the scatterer in order to do this.

The aim of this dissertation is to use MATLAB to develop 'black box' software to solve the inverse problem for acoustic scattering in two dimensions. Given discrete data on the total field due to acoustic wave scattering from an unknown object, the software will locate the edges of the object, and so construct an image of the scatterer.

Chapter 2

Background

2.1 The Helmholtz Equation

Consider the complex scalar field $\Psi(\mathbf{x}, t) \in C^2(\mathbb{R}^m) \cap C^2(\mathbb{R})$ for $m = 2, 3$, for a wave propagating with speed $c > 0$. Then Ψ satisfies the wave equation

$$\Delta\Psi = \frac{1}{c^2}\Psi_{tt} \tag{2.1}$$

We can look for *time-harmonic solutions* of (2.1), that is, solutions of the form

$$\Psi(\mathbf{x}, t) = \phi(\mathbf{x})e^{-i\omega t}$$

with angular frequency $\omega > 0$. Substituting this form into (2.1) we obtain for $\phi(\mathbf{x})$ the *Helmholtz equation*

$$(\Delta + \kappa^2)\phi(\mathbf{x}) = 0 \qquad \mathbf{x} \in \mathbb{R}^m \tag{2.2}$$

for *wave number* $\kappa = \omega/c > 0$. From now on, the term *field* will refer only to the spatial part $\phi(\mathbf{x})$ of the time-harmonic field.

We may choose to find solutions for $\phi(\mathbf{x})$ that model the field of *radiating waves*, by definition, solutions for $\mathbf{x} \in \mathbb{R}^m$ that satisfy the *Sommerfeld radiation condition*

$$\lim_{r\to\infty} r^{\frac{m-1}{2}} \left(\frac{\partial\phi}{\partial r} - i\kappa\phi \right) = 0 \tag{2.3}$$

where $r := |\mathbf{x}|, m = 2, 3$.

Define the function $\Phi(\mathbf{x}, \mathbf{z})$, $\mathbf{x} \in \mathbb{R}^m \backslash \{\mathbf{z}\}$, dependent upon m, by

$$\Phi(\mathbf{x}, \mathbf{z}) := \frac{i}{4} H_0^{(1)}(\kappa|\mathbf{x} - \mathbf{z}|) \text{ for } m = 2 \tag{2.4}$$

$$\Phi(\mathbf{x}, \mathbf{z}) := \frac{1}{4\pi} \frac{e^{i\kappa|\mathbf{x}-\mathbf{z}|}}{|\mathbf{x} - \mathbf{z}|} \text{ for } m = 3 \tag{2.5}$$

where $H_0^{(1)}$ is the Hankel function of the first kind, of order zero. Then in each case for m, $\phi(\mathbf{x}) = \Phi(\mathbf{x}, \mathbf{z})$ satisfies (2.3) and (2.2) (modulo a constant) except at $\mathbf{x} = \mathbf{z}$, and is called the *fundamental solution to the Helmholtz equation.*

We can model the field corresponding to a *plane wave* moving in some direction $\hat{\mathbf{d}}$ (with $|\hat{\mathbf{d}}| = 1$) by the function

$$\phi(\mathbf{x}) = e^{i\kappa \mathbf{x} \cdot \hat{\mathbf{d}}} \tag{2.6}$$

This is a solution of (2.2) (modulo a constant), but since the corresponding wave is plane and not radiating, (2.3) is not satisfied.

2.2 Hankel Functions

The Hankel functions are a specific linear combination of Bessel and Neuman functions, namely

$$H_p^{(1,2)} = J_p(x) \pm iY_p(x) \qquad p, x \in \mathbb{R} \tag{2.7}$$

respectively, for the Bessel function $J_p(x)$ and Neuman function $Y_p(x)$. $J_p(x)$ is a series solution to Bessel's equation

$$x^2y'' + xy' + (x^2 - p^2)y = 0$$

obtainable using Frobenius' method [2, pp.509-512], and can be written down as

$$J_{\pm p} = \sum_{n=0}^{\infty} \frac{(-1)^n}{\Gamma(n+1)\Gamma(n \pm p + 1)} \left(\frac{x}{2}\right)^{2n \pm p} \tag{2.8}$$

which converges for all $x \in \mathbb{R}$. The Neuman function Y_p is a linear combination of Bessel functions

$$Y_p(x) = \frac{\cos(\pi p)J_p(x) - J_{-p}(x)}{\sin(\pi p)} \tag{2.9}$$

and therefore Y_p is also a solution to Bessel's equation. Note that $Y_p(x)$ has the indeterminate form $0/0$ for $p \in \mathbb{Z}$. So for integral p we define $Y_p(x)$ by

$$Y_p := \lim_{q \to p} Y_q \qquad p \in \mathbb{Z}$$

which leads us [1, p.97] to the result

$$Y_p = \frac{1}{\pi}\left[\frac{\partial J_q(x)}{\partial q} - (-1)^q \frac{\partial J_{-q}(x)}{\partial q}\right]_{q=p} \qquad p \in \mathbb{Z}$$

and $(i/4)H_0^1$ under this definition solves (2.2). $Y_p(x)$ with $p \in \mathbb{Z}$ has a logarithmic pole at $x = 0$ (and so too the imaginary part of $H_p^{(1,2)} p \in \mathbb{Z}$, see figures (2.1), (2.2)).

Since it will be needed later, we prove following relation between the Hankel functions.

Theorem 1 *The Hankel functions satisfy the recursion relation*

$$\frac{d}{dx}\{H_p^{(1,2)}(x)\} = \frac{p}{x}H_p^{(1,2)}(x) - H_{p+1}^{(1,2)}(x) \tag{2.10}$$

Proof We first prove that the bessel function J_p satisfies the above relation. Since (2.8) converges for all x, then

$$\begin{aligned}
\frac{d}{dx}\{J_p(x)\} &= \sum_{n=0}^{\infty} \frac{(-1)^n}{\Gamma(n+p+1)\Gamma(n+1)} \frac{d}{dx}\left(\frac{x}{2}\right)^{2n+p} \\
&= \sum_{n=0}^{\infty} \frac{(p+2n)(-1)^n x^{2n+p-1}}{\Gamma(n+p+1)\Gamma(n+1)2^{2n+p}} \\
&= \frac{p}{x}J_p + \sum_{n=0}^{\infty} \frac{n(-1)^n}{\Gamma(n+p+1)\Gamma(n+1)}\left(\frac{x}{2}\right)^{2n+p-1} \\
&= \frac{p}{x}J_p + \sum_{n=1}^{\infty} \frac{n(-1)^n}{\Gamma(n+p+1)\Gamma(n+1)}\left(\frac{x}{2}\right)^{2n+p-1} \qquad \text{since the first term is zero} \\
&= \frac{p}{x}J_p - \sum_{\nu=0}^{\infty} \frac{(\nu+1)(-1)^\nu}{\Gamma(\nu+(p+1)+1)\Gamma(\nu+2)}\left(\frac{x}{2}\right)^{2\nu+(p+1)} \qquad \text{where } \nu := n-1 \\
&= \frac{p}{x}J_p - \sum_{\nu=0}^{\infty} \frac{(\nu+1)(-1)^\nu}{(\nu+1)\Gamma(\nu+(p+1)+1)\Gamma(\nu+1)}\left(\frac{x}{2}\right)^{2\nu+(p+1)}
\end{aligned}$$

$$= \frac{p}{x}J_p - J_{p+1}$$

It follows that since Y_p is a linear combination of Bessel functions and $H_p^{(1,2)}$ is a linear combination of Bessel and Neuman functions, then they too satisfy the relation. $\square$

Consider the modified Bessel function of the second kind $K_p(x)$ given by

$$K_p(x) = \frac{\sqrt{\pi}}{\Gamma(p+\frac{1}{2})}\left(\frac{x}{2}\right)^p \int_{-1}^{\infty} e^{-xt}(t^2-1)^{p-\frac{1}{2}}dt \qquad p > -\frac{1}{2}, x > 0$$

In [1] Bell shows that under the change of variables $t = 1 + u/x$, $K_p(x)$ becomes

$$K_p(x) = \frac{\sqrt{\pi}}{\Gamma(p+\frac{1}{2})}\left(\frac{2}{x}\right)^{-\frac{1}{2}} \frac{1}{x}e^{-x}\int_0^{\infty} e^{-u}u^{p-\frac{1}{2}}\left(1+\frac{u}{2x}\right)^{p-\frac{1}{2}}du$$

By Taylor's Theorem (with the Lagrange form of the remainder), for all $q \in \mathbb{R}$, and $|\mathbf{x}| < 1$ we have that

$$(1+x)^q = 1 + qx + \frac{q(q-1)}{2!}x^2 + \ldots + \frac{q(q-1)(p-2)\ldots(q-N+1)}{N!}x^N + R_{N+1}(x) \quad (2.11)$$

where

$$R_{N+1}(x) = \frac{q(q-1)...(q-N)}{(N+1)!}(1+\zeta)^{q-N-1}x^{N+1} = O(x^{N+1}) \quad (2.12)$$

for some ζ between 0 and x (i.e. $\zeta \in (0,x)$ for $x > 0$, and $\zeta \in (x,0)$ for $x < 0$. Then, for $|x|$ sufficiently large (i.e $|x| > |u/2|$) we have that

$$\left(1+\frac{u}{2x}\right)^{p-\frac{1}{2}} = 1 + R_1(\frac{u}{2x})$$

and so

$$\begin{aligned} K_p(x) &= \frac{\sqrt{\pi}}{\Gamma(p+\frac{1}{2})}\left(\frac{2}{x}\right)^{-\frac{1}{2}} \frac{1}{x}e^{-x}\{\int_0^{\infty} e^{-u}u^{p-\frac{1}{2}}du + \int_0^{\infty} R_1(\frac{u}{2x})e^{-u}u^{p-\frac{1}{2}}du\} \\ &= \frac{\sqrt{\pi}}{\Gamma(p+\frac{1}{2})}\left(\frac{2}{x}\right)^{-\frac{1}{2}} \frac{1}{x}e^{-x}\{\Gamma(p+\frac{1}{2}) + O(\frac{1}{x})\} \\ &= \sqrt{\frac{\pi}{2x}}\{1+O(\frac{1}{x})\} \end{aligned}$$

i.e. $K_p(x) \sim \sqrt{\pi/2x}$ as $|x| \to \infty$.

It is possible [1, p.129] to express $H_p^{(1)}(x)$ as

$$H_p^{(1)}(x) = \frac{2}{\pi} e^{-i\frac{\pi}{2}(p+1)} K_p(-ix) \tag{2.13}$$

and so using the above result we have that as $|x| \to \infty$

$$H_p^{(1)}(x) = \frac{2}{\pi} e^{-i\frac{\pi}{2}(p+1)} \sqrt{\frac{\pi}{-2ix}} \{1 + O(\frac{1}{x})\}$$

which upon rearranging gives (for $p > -1/2$)

$$H_p^{(1)}(x) = \sqrt{\frac{2}{\pi x}} e^{i\{x-(p+\frac{1}{2})\frac{\pi}{2}\}} \{1 + O(\frac{1}{x})\} \qquad \text{as } |x| \to \infty \tag{2.14}$$

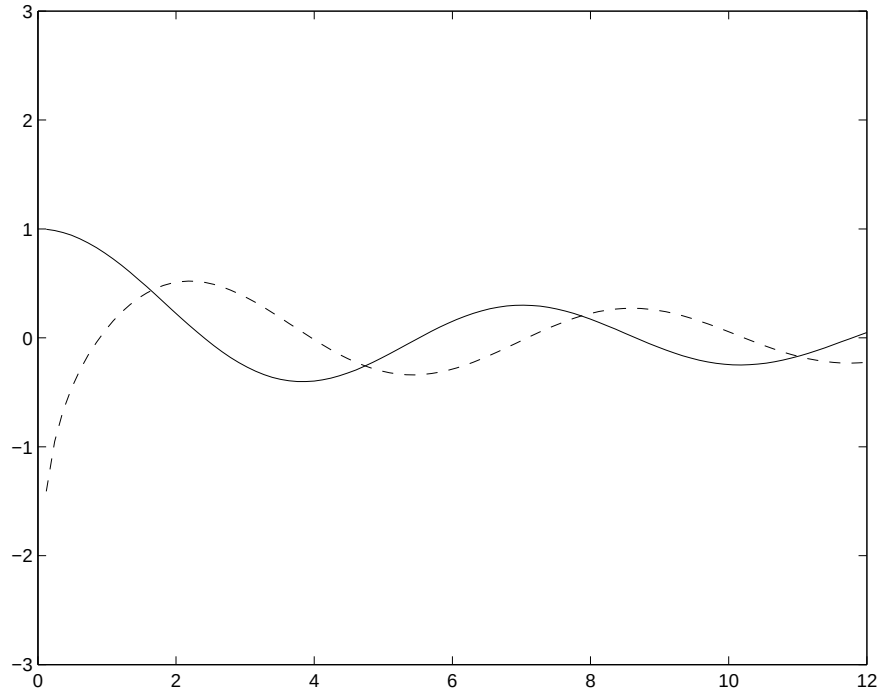

Figure 2.1: Real (solid) and imaginary (dashed) parts of $H_0^{(1)}(x)$

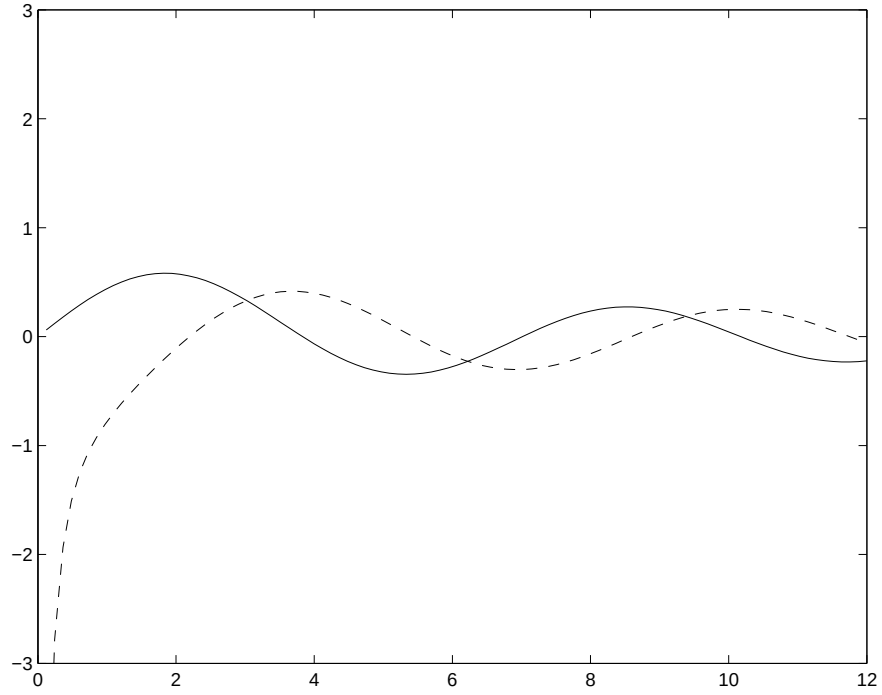

Figure 2.2: Real (solid) and imaginary (dashed) parts of $H_1^{(1)}(x)$

Chapter 3

Acoustic Scattering

3.1 The Direct Scattering Problem

We suppose that the interior of the scatterer occupies a region $D \subset \mathbb{R}^m$, where D is an open set bounded by ∂D, and $\mathbb{R}^m \backslash \bar{D}$ is connected where $\bar{D}$ denotes the closure of D (i.e. $\bar{D} := D \cup \partial D$). We require that ∂D is of class C^2 (i.e. ∂D has continuous curvature).

Denote by $v(\mathbf{x})$, $\mathbf{x} \in \mathbb{R}^m \backslash \bar{D}$ a solution to (2.2) on the exterior of the scatterer. Then we can require that $v(\mathbf{x})$ satisfies the *exterior acoustic Dirichlet problem.*

Exterior Acoustic Dirichlet Problem (EADP) *Given Dirichlet data $g \in C(\partial D)$, find $v(\mathbf{x}) \in C^2(\mathbb{R}^m \backslash \bar{D}) \cap C(\mathbb{R}^m \backslash D)$ such that*

$$\begin{aligned} (\Delta + \kappa^2) v(\mathbf{x}) &= 0 \qquad \mathbf{x} \in \mathbb{R}^m \backslash \bar{D} \\ v(\mathbf{x}) &= g(\mathbf{x}) \qquad \mathbf{x} \in \partial D \\ \lim_{r \to \infty} r^{\frac{m-1}{2}} \left(\frac{\partial v}{\partial r} - i\kappa v \right) &= 0 \qquad \text{for } r = |\mathbf{x}| \end{aligned}$$

Theorem 2 *The EADP has a unique solution.*

Proof See [3, p.48] □

We turn our attention to the practical problem of acoustic wave scattering. On the exterior of the scatterer there exists a field, which is the sum of the field corresponding to an incident wave, and the field corresponding to the scattered wave. In particular, we consider the case when the incident wave is plane.

For time-harmonic incident plane waves with $\kappa = \omega/c > 0$ travelling in direction $\hat{\mathbf{d}} \in \Omega := \{\mathbf{v} \in \mathbb{R}^m : |\mathbf{v}| = 1\}$ we denote

$$u^i(\mathbf{x}, \hat{\mathbf{d}}) := e^{i\kappa \mathbf{x}\cdot\hat{\mathbf{d}}} \qquad \mathbf{x} \in \mathbb{R}^m \backslash \bar{D} \tag{3.1}$$

which models the corresponding field, and solves the Helmholtz equation.

We denote the total field (which one might observe with instrumentation) measured on the exterior of the scatterer to be

$$u^t(\mathbf{x}, \hat{\mathbf{d}}) \qquad \mathbf{x} \in \mathbb{R}^m \backslash \bar{D}$$

and in this way we may define the field of the scattered wave to be

$$u^s(\mathbf{x}, \hat{\mathbf{d}}) := u^t(\mathbf{x}, \hat{\mathbf{d}}) - u^i(\mathbf{x}, \hat{\mathbf{d}}) \qquad \mathbf{x} \in \mathbb{R}^m \backslash \bar{D}$$

Finally, we set the scatterer to be *sound-soft*. That is, the total field vanishes on the surface of the scatterer

$$u^t(\mathbf{x}, \hat{\mathbf{d}}) = u^i(\mathbf{x}, \hat{\mathbf{d}}) + u^s(\mathbf{x}, \hat{\mathbf{d}}) = 0 \qquad \mathbf{x} \in \partial D \tag{3.2}$$

Recall that the direct scattering problem is to use knowledge of the scatterer and the field of the incident wave, to find the field of the scattered wave on the exterior of the object (and therefore the total field). Armed with the above definitions, we can now formulate this problem mathematically.

Direct Acoustic Scattering Problem (DASP) *For $\bar{D}$ and κ defined as above, find $u^s(\mathbf{x}, \hat{\mathbf{d}}) \in C^2(\mathbb{R}^m \backslash \bar{D}) \cap C(\mathbb{R}^m \backslash D)$ that satisfies*

$$(\Delta + \kappa^2) u^s(\mathbf{x}, \hat{\mathbf{d}}) = 0 \qquad \mathbf{x} \in \mathbb{R}^m \backslash \bar{D}$$

with the sound-soft boundary condition

$$u^s(\mathbf{x}, \hat{\mathbf{d}}) = -u^i(\mathbf{x}, \hat{\mathbf{d}}) \qquad \mathbf{x} \in \partial D$$

and which satisfies the Sommerfeld radiation condition

$$\lim_{r\to\infty} r^{\frac{m-1}{2}} \left(\frac{\partial u^s}{\partial r} - i\kappa u^s \right) = 0$$

for $r = |\mathbf{x}|$.

It is clear that the DASP is a special case of the EADP with $g = -u^i(\mathbf{x}, \hat{\mathbf{d}})$, and therefore a unique solution exists.

3.2 Solution

We present the solution to the direct problem in the form of an integral equation [3, p.42]. For continuous density function $\varphi \in C(\partial D)$ the solution to the direct acoustic scattering problem is given by

$$u^s(\mathbf{x}, \hat{\mathbf{d}}) = \int_{\partial D} \left(\frac{\partial \Phi(\mathbf{x}, \mathbf{z})}{\partial \hat{\mathbf{n}}(\mathbf{z})} - i\Phi(\mathbf{x}, \mathbf{z}) \right) \varphi(\mathbf{z}) dS(\mathbf{z}) \qquad \mathbf{x} \in \mathbb{R}^m \backslash \bar{D} \tag{3.3}$$

where φ is a solution to the boundary integral equation

$$(\mathcal{I} + \mathcal{K} - i\mathcal{S})\varphi = -2u^i(\mathbf{x}, \hat{\mathbf{d}})|_{\partial D} \tag{3.4}$$

for the *single-layer operator* $\mathcal{S}$ defined by

$$(\mathcal{S}\varphi)(\mathbf{x}) := 2 \int_{\partial D} \Phi(\mathbf{x}, \mathbf{z}) \varphi(\mathbf{z}) dS(\mathbf{z}) \qquad \mathbf{x} \in \partial D \tag{3.5}$$

the *double-layer operator* $\mathcal{K}$ defined by

$$(\mathcal{K}\varphi)(\mathbf{x}) := 2 \int_{\partial D} \frac{\partial \Phi(\mathbf{x}, \mathbf{z})}{\partial \hat{\mathbf{n}}(\mathbf{z})} \varphi(\mathbf{z}) dS(\mathbf{z}) \qquad \mathbf{x} \in \partial D \tag{3.6}$$

and where $\mathcal{I}$ is the identity operator and $\hat{\mathbf{n}}(\mathbf{z})$ is the outward normal vector to the surface at $\mathbf{z} \in \partial D$.

3.3 2D Numerical Implementation

We solve the direct scattering problem by approximating the single-layer and double-layer operators by matrix operators, and so reduce the problem to solving a linear system of equations.

We consider the boundary ∂D of our scatterer to be parameterised by some 2π periodic vector valued function $\mathbf{z} : \mathbb{R} \to \mathbb{R}^2$, such that

- (i) $\partial D = \{\mathbf{z}(\theta) : \theta \in \mathbb{R}\}$
- (ii) $\mathbf{z}(a) = \mathbf{z}(b) \iff a - b$ is a multiple of 2π
- (iii) $|a - b| \leq \epsilon \implies c(\epsilon)|a - b| \leq |\mathbf{z}(b) - \mathbf{z}(a)| \leq C(\epsilon)|a - b|$ for constants $c(\epsilon), C(\epsilon) \in \mathbb{R}$
- (iv) $\mathbf{z} \in C^2(\mathbb{R})$

By (iii) we can consider the line element dS along ∂D at $\mathbf{z}(\theta)$ to be the limit

$$dS = \lim_{d\theta \to 0} |\mathbf{z}(\theta + d\theta) - \mathbf{z}(\theta)|$$

Then we see that

$$dS = \lim_{d\theta \to 0} |d\theta \frac{\mathbf{z}(\theta + d\theta) - \mathbf{z}(\theta)}{d\theta}| = d\theta |\mathbf{z}'(\theta)|$$

and so the single-layer operator is given by

$$\begin{aligned} (\mathcal{S}\varphi)(\mathbf{x}) &= 2\int_{\partial D} \Phi(\mathbf{x}, \mathbf{z})\varphi(\mathbf{z}) dS(\mathbf{z}) \qquad \mathbf{x} \in \partial D \\ &= 2\int_0^{2\pi} \Phi(\mathbf{x}, \mathbf{z}(\theta))\varphi(\mathbf{z}(\theta))|\mathbf{z}'(\theta)| d\theta \end{aligned}$$

Since we are integrating over the period of the integrand, we will approximate this integral using the composite trapezoidal rule, which though only a first order method, can be found to achieve higher orders of accuracy for periodic integrands. Consider a function $f \in C^\infty(0, 2\pi)$, and partition the interval $(0, 2\pi)$ into $N-1$ intervals of length h such that $(0, 2\pi) = \bigcup_{n=0}^{N-1}(nh, (n+1)h)$. Then for $f_j := f(jh)$ we have (by the *Euler-Maclaurin summation formula*)

$$\int_0^{2\pi} f(x)dx = h\frac{f_0}{2} + h\frac{f_N}{2} + h\sum_{j=1}^{N-1} f_j - \frac{B_2}{2!}h^2(f'_N - f'_0) - \frac{B_4}{4!}h^4(f_N^{(3)} - f_0^{(3)}) - .....$$

where B_i is the i^{th} Bernoulli number. Then for $f(0) = f(2\pi)$ we have that $f_0^{(i)} = f_N^{(i)}$ for $i = 0, 1, 2, ...$, and so

$$\int_0^{2\pi} f(x)dx = h\sum_{j=0}^{N-1} f_j + rem = h\sum_{j=1}^{N} f_j + rem$$

where $rem = o(h^M)$ for all M.

Since $\mathbf{z}(\theta)$ is 2π periodic in θ, then $\Phi(\mathbf{x}, \mathbf{z}(\theta))$ and $\varphi(\mathbf{z}(\theta))$ are both 2π periodic functions in θ, and so for the partition $(0, 2\pi) = \bigcup_{n=0}^{N-1}(n\delta\theta, (n+1)\delta\theta)$ and where $\theta_n = n\delta\theta$ (with $\delta\theta = 2\pi/N$) we can approximate the single-layer potential by

$$\begin{aligned} (\mathcal{S}\varphi)(\mathbf{x}) &= 2\delta\theta \sum_{n=1}^{N} \Phi(\mathbf{x}, \mathbf{z}(\theta_n))\varphi(\mathbf{z}(\theta_n))|\mathbf{z}'(\theta_n)| + rem_{\mathcal{S}}(N) \\ \text{where } \Phi(\mathbf{x}, \mathbf{z}(\theta_n)) &= \frac{i}{4}H_0^{(1)}(\kappa|\mathbf{x} - \mathbf{z}(\theta_n)|) \qquad \mathbf{x} \neq \mathbf{z}(\theta_n) \end{aligned}$$

In this way we discretise the boundary ∂D by the ordered set of points $Z = (\mathbf{z}(\theta_n))_{n=0}^{N-1}$. Clearly the integrand of $(\mathcal{S}\phi)(\mathbf{x})$ does not have the continuity properties required by the Euler-Maclaurin formula, owing to the logarithmic pole at $\mathbf{x} = \mathbf{z}$, and so it is unclear as to how $rem_{\mathcal{S}}(N)$ will converge as $N \to \infty$.

Here we use Theorem 1 to compute the outward normal derivative to $\Phi(\mathbf{x}, \mathbf{z})$

$$\begin{aligned}
\frac{\partial}{\partial \hat{\mathbf{n}}}\Phi(\mathbf{x},\mathbf{z}) &= \frac{i}{4}\frac{\partial}{\partial \hat{\mathbf{n}}}H_0^1(\kappa|\mathbf{x}-\mathbf{z}|) \\
&= -\frac{i\kappa}{4}H_1^1(\kappa|\mathbf{x}-\mathbf{z}|)\hat{\mathbf{n}}(\mathbf{z})\cdot\nabla_{\mathbf{z}}\{|\mathbf{x}-\mathbf{z}|\} \\
&= \frac{i\kappa\hat{\mathbf{n}}(\mathbf{z})\cdot(\mathbf{x}-\mathbf{z})}{4|\mathbf{x}-\mathbf{z}|}H_1^1(\kappa|\mathbf{x}-\mathbf{z}|)
\end{aligned}$$

and so similarly we obtain an approximation to the double-layer potential in 2D

$$\begin{aligned}
(\mathcal{K}\varphi)(\mathbf{x}) &= 2\delta\theta\sum_{n=1}^{N}\frac{\partial\Phi(\mathbf{x},\mathbf{z}(\theta_n))}{\partial\hat{\mathbf{n}}(\mathbf{z}(\theta_n))}\varphi(\mathbf{z}(\theta_n))|\mathbf{z}'(\theta_n)| + rem_{\mathcal{K}}(N) \\
\text{where } \frac{\partial\Phi(\mathbf{x},\mathbf{z}(\theta_n))}{\partial\hat{\mathbf{n}}(\mathbf{z}(\theta_n))} &= \frac{i\kappa\hat{\mathbf{n}}(\mathbf{z}(\theta_n))\cdot(\mathbf{x}-\mathbf{z}(\theta_n))}{4|\mathbf{x}-\mathbf{z}(\theta_n)|}H_1^1(\kappa|\mathbf{x}-\mathbf{z}(\theta_n)|) \qquad \mathbf{x}\neq\mathbf{z}(\theta_n)
\end{aligned}$$

We now introduce the notation $\varphi_n := \varphi(\mathbf{z}(\theta_n))$, and let $Q := (\mathbf{q}_i)_{i=1}^{M} \subset \mathbb{R}^2\backslash\bar{D}$ be an ordered set of points at which we wish to solve the direct scattering BVP. Define the $M \times N$ matrices

$$\begin{aligned}
S_Q(m,n) &:= \delta\theta\frac{i}{4}H_0^{(1)}(\kappa|\mathbf{q}_m-\mathbf{z}(\theta_n)|)|\mathbf{z}'(\theta_n)| \\
S_Z(m,n) &:= 2\delta\theta\frac{i}{4}H_0^{(1)}(\kappa|\mathbf{z}(\theta_m)-\mathbf{z}(\theta_n)|)|\mathbf{z}'(\theta_n)| \qquad m\neq n \\
&:= 2\delta\theta\frac{ic_+}{4}H_0^{(1)}(\kappa|\mathbf{z}(\theta_m)-\mathbf{z}(\theta_{n+1})|)|\mathbf{z}'(\theta_{n+1})| \\
&\quad +2\delta\theta\frac{ic_-}{4}H_0^{(1)}(\kappa|\mathbf{z}(\theta_m)-\mathbf{z}(\theta_{n-1})|)|\mathbf{z}'(\theta_{n-1})| \qquad m=n
\end{aligned}$$

and similarly

$$
\begin{aligned}
K_Q(m,n) &:= \delta\theta \frac{i\kappa \hat{\mathbf{n}}(\mathbf{z}(\theta_n)) \cdot (\mathbf{q}_m - \mathbf{z}(\theta_n))}{4|\mathbf{q}_m - \mathbf{z}(\theta_n)|} H_1^{(1)}(\kappa|\mathbf{q}_m - \mathbf{z}(\theta_n)|)|\mathbf{z}'(\theta_n)| \\
K_Z(m,n) &:= 2\delta\theta \frac{i\kappa \hat{\mathbf{n}}(\mathbf{z}(\theta_n)) \cdot (\mathbf{z}_m - \mathbf{z}(\theta_n))}{4|\mathbf{z}_m - \mathbf{z}(\theta_n)|} H_1^{(1)}(\kappa|\mathbf{z}(\theta_m) - \mathbf{z}(\theta_n)|)|\mathbf{z}'(\theta_n)| \qquad m \neq n \\
&:= 2\delta\theta c_+ \frac{i\kappa \hat{\mathbf{n}}(\mathbf{z}(\theta_{n+1})) \cdot (\mathbf{z}_m - \mathbf{z}(\theta_{n+1}))}{4|\mathbf{z}_m - \mathbf{z}(\theta_{n+1})|} H_1^{(1)}(\kappa|\mathbf{z}(\theta_m) - \mathbf{z}(\theta_{n+1})|)|\mathbf{z}'(\theta_{n+1})| \\
&\quad + 2\delta\theta c_- \frac{i\kappa \hat{\mathbf{n}}(\mathbf{z}(\theta_{n-1})) \cdot (\mathbf{z}_m - \mathbf{z}(\theta_{n-1}))}{4|\mathbf{z}_m - \mathbf{z}(\theta_{n-1})|} H_1^{(1)}(\kappa|\mathbf{z}(\theta_m) - \mathbf{z}(\theta_{n-1})|)|\mathbf{z}'(\theta_{n-1})| \\
&\qquad\qquad\qquad\qquad\qquad\qquad\qquad\qquad\qquad\qquad\qquad\qquad\qquad\qquad\qquad\qquad m = n
\end{aligned}
$$

for coefficients

$$
\begin{aligned}
c_+ &:= \frac{|\mathbf{z}(\theta_n) - \mathbf{z}(\theta_{n+1})|}{|\mathbf{z}(\theta_{n+1}) - \mathbf{z}(\theta_{n-1})|} \\
c_- &:= \frac{|\mathbf{z}(\theta_n) - \mathbf{z}(\theta_{n-1})|}{|\mathbf{z}(\theta_{n+1}) - \mathbf{z}(\theta_{n-1})|}
\end{aligned}
$$

where $\theta_{N+1} := \theta_1$ and $\theta_0 := \theta_N$. Let $w^s(\mathbf{x}, \hat{\mathbf{d}})$ be our numerical solution for $u^s(\mathbf{x}, \hat{\mathbf{d}})$ for some $\hat{\mathbf{d}} \in \Omega$. Then, upon defining the vectors

$$
\begin{aligned}
\vec{u}^i_{\hat{\mathbf{d}}} &:= (u^i(\mathbf{z}(\theta_1), \hat{\mathbf{d}}), ..., u^i(\mathbf{z}(\theta_N), \hat{\mathbf{d}})^T \\
\vec{w}^s_{\hat{\mathbf{d}}} &:= (w^s(\mathbf{z}(\theta_1), \hat{\mathbf{d}}), ..., w^s(\mathbf{z}(\theta_N), \hat{\mathbf{d}})^T
\end{aligned}
$$

by (3.4) and (3.3) we can compute $w^s(\mathbf{x}, \hat{\mathbf{d}})$ as

$$
\vec{w}^s_{\hat{\mathbf{d}}} = -2(K_Q - iS_Q)(I + K_Z - iS_Z)^{-1}\vec{u}^i_{\hat{\mathbf{d}}} \tag{3.7}
$$

3.4 Numerical Results

Here we consider ∂D to be 'peanut shaped' (see figure 3.1), a specific hippopede given by

$$r = \frac{3}{2} - \sin^2\theta$$

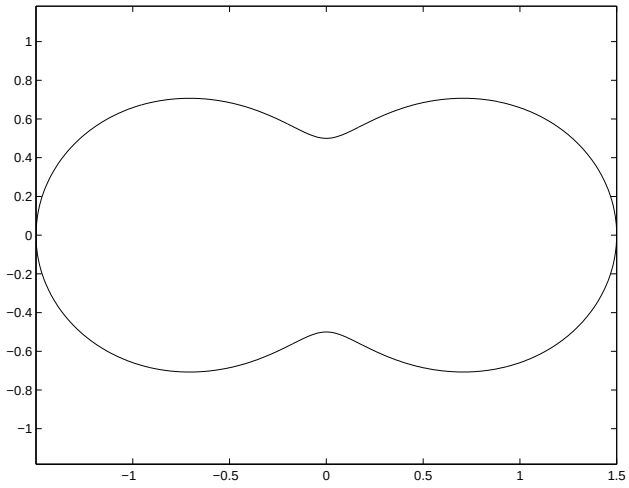

Figure 3.1: 'Peanut' defined by $r = 3/2 - \sin^2\theta$

We can test the accuracy of our numerical method by applying it to the exterior acoustic Dirichlet problem. We have already seen that the direct acoustic scattering problem is a special case of the EADP, and so

$$v(\mathbf{x}) = \int_{\partial D} \left(\frac{\partial \Phi(\mathbf{x}, \mathbf{z})}{\partial \hat{\mathbf{n}}(\mathbf{z})} - i\Phi(\mathbf{x}, \mathbf{z}) \right) \varphi(\mathbf{z}) dS(\mathbf{z})$$

solves the EADP iff

$$(\mathcal{I} + \mathcal{K} - i\mathcal{S})\varphi = 2g$$

for integral operators $\mathcal{K}$, and $\mathcal{S}$ as defined earlier, and boundary data $g \in C(\partial D)$.

If we set $g = \Phi(\mathbf{x}, \mathbf{z}^*)$ for some particular point $\mathbf{z}^* \in D$, then $v = \Phi(\mathbf{x}, \mathbf{z}^*)$ is clearly the solution to the EADP. Then, if we define

$$\vec{u}^i_{\mathbf{z}^*} := (\Phi(\mathbf{z}(\theta_1), \mathbf{z}^*), ..., \Phi(\mathbf{z}(\theta_N), \mathbf{z}^*))^T$$
$$\vec{\psi}_{\mathbf{z}^*} := (\psi_1, ..., \psi_M)^T$$

(and so ψ_j is our approximation to $\Phi(\mathbf{x_j}, \mathbf{0})$) and apply our approximation to calculating

$$\vec{\psi}_{\mathbf{z}^*} = -2(K_Q - iS_Q)(I + K_Z - iS_Z)^{-1}\vec{u}^i_{\mathbf{z}^*}$$

we can look at how $\psi_j \to \Phi(\mathbf{x}_j, \mathbf{z}^*)$ as $N \to \infty$ (for $\mathbf{x}_j \in \mathbb{R}^2 \backslash \bar{D}$) (see table). Clearly, we only achieve first order accuracy, though the exercise serves as a test to show that the numerical method converges to the correct solution. Our numerical solution is illustrated in figure 8.1.

N	$\lvert\psi_j - \Phi(\mathbf{x}_j, \mathbf{0})\rvert / \lvert\Phi(\mathbf{x}_j, \mathbf{0})\rvert$	*Estimated Order of Convergence*
5	1.401259×10^{0}	
10	2.944734×10^{0}	-1.071413×10^{0}
20	4.952713×10^{-1}	2.5718464×10^{0}
40	8.843449×10^{-2}	2.4855381×10^{0}
80	6.669067×10^{-2}	4.0712421×10^{-1}
160	3.265709×10^{-2}	1.0300886×10^{0}
320	1.598911×10^{-2}	1.0303071×10^{0}
640	7.912897×10^{-3}	1.0148113×10^{0}
1280	3.940064×10^{-3}	1.0059869×10^{0}

Table 3.1: Convergence of numerical method for direct problem (at $\mathbf{x}_j = (-3, 3)^T$)

Chapter 4

The Point Source Method

4.1 Asymptotic Behaviour

If we set the boundary condition for the EADP to $g = -\Phi(\mathbf{x}, \mathbf{z})$ where $|\mathbf{z}|$ is large (and therefore we model scattering of waves due to a point source far away from the scatterer), we expect the solution to resemble the field of waves scattered due to a plane wave incident with direction $-\hat{\mathbf{z}} = -\mathbf{z}/|\mathbf{z}|$. This is more clearly seen if we look at the asymptotic behaviour of $\Phi(\mathbf{x}, \mathbf{z})$ as $|\mathbf{z}| \to \infty$. From (2.14) we have that

$$\begin{aligned}\Phi(\mathbf{x}, \mathbf{z}) &= \frac{i}{\sqrt{8\pi\kappa|\mathbf{x}-\mathbf{z}|}} e^{i(\kappa|\mathbf{x}-\mathbf{z}|-\frac{\pi}{4})}\{1 + O(\frac{1}{|\mathbf{x}-\mathbf{z}|})\} \text{ as } |\mathbf{x}-\mathbf{z}| \to \infty \\ &= \frac{(1+i)}{4\sqrt{\pi\kappa|\mathbf{x}-\mathbf{z}|}} e^{i\kappa|\mathbf{x}-\mathbf{z}|}\{1 + O(\frac{1}{|\mathbf{x}-\mathbf{z}|})\} \text{ as } |\mathbf{x}-\mathbf{z}| \to \infty\end{aligned}$$

We can look at the case when $|\mathbf{x}-\mathbf{z}| \to \infty$ for fixed $\mathbf{x}$. By (2.11) and (2.12) we have

$$\begin{aligned}|\mathbf{x}-\mathbf{z}| &= \sqrt{|\mathbf{x}|^2 - 2\mathbf{x}\cdot\mathbf{z} + |\mathbf{z}|^2} \\ &= |\mathbf{z}|\sqrt{1 - 2\frac{\mathbf{x}\cdot\hat{\mathbf{z}}}{|\mathbf{z}|} + \frac{|\mathbf{x}|^2}{|\mathbf{z}|^2}} \\ &= |\mathbf{z}|\{1 - \frac{\mathbf{x}\cdot\hat{\mathbf{z}}}{|\mathbf{z}|} + \frac{1}{2}\frac{|\mathbf{x}|^2}{|\mathbf{z}|^2} + R_2(\mathbf{x}, \mathbf{z})\} \qquad \text{for } |\mathbf{z}| > \epsilon \text{ for some } \epsilon > 0\end{aligned}$$

for remainder term

$$R_2(\mathbf{x}, \mathbf{z}) = -\frac{1}{8}\left(1 - 2\frac{\mathbf{x}\cdot\hat{\zeta}}{|\zeta|} + \frac{|\mathbf{x}|^2}{|\zeta|^2}\right)^{-\frac{3}{2}}\left(-2\frac{\mathbf{x}\cdot\hat{\mathbf{z}}}{|\mathbf{z}|} + \frac{|\mathbf{x}|^2}{|\mathbf{z}|^2}\right)^2$$

for some ζ such that

$$\begin{aligned} -2\frac{\mathbf{x}\cdot\hat{\zeta}}{|\zeta|}+\frac{|\mathbf{x}|^2}{|\zeta|^2} &\in \left(0,-2\frac{\mathbf{x}\cdot\hat{\mathbf{z}}}{|\mathbf{z}|}+\frac{|\mathbf{x}|^2}{|\mathbf{z}|^2}\right) \text{ if } -2\frac{\mathbf{x}\cdot\hat{\mathbf{z}}}{|\mathbf{z}|}+\frac{|\mathbf{x}|^2}{|\mathbf{z}|}^2>0 \\ &\in \left(-2\frac{\mathbf{x}\cdot\hat{\mathbf{z}}}{|\mathbf{z}|}+\frac{|\mathbf{x}|^2}{|\mathbf{z}|^2},0\right) \text{ if } -2\frac{\mathbf{x}\cdot\hat{\mathbf{z}}}{|\mathbf{z}|}+\frac{|\mathbf{x}|^2}{|\mathbf{z}|^2}<0 \end{aligned}$$

when $|\mathbf{z}|>\epsilon$. Then for $|\mathbf{z}|$ sufficiently large

$$\begin{aligned} \Phi(\mathbf{x},\mathbf{z}) &= \frac{(1+i)}{4\sqrt{\pi\kappa|\mathbf{x}-\mathbf{z}|}}\exp\{i\kappa|\mathbf{z}|\}\exp\{-i\kappa\mathbf{x}\cdot\hat{\mathbf{z}}\}\exp\{i\kappa\frac{1}{2}\frac{|\mathbf{x}|^2}{|\mathbf{z}|}+i\kappa|\mathbf{z}|R_2(\mathbf{x},\mathbf{z})\} \\ &\quad\times\{1+O(\frac{1}{|\mathbf{x}-\mathbf{z}|})\} \\ &= \frac{(1+i)e^{i\kappa|\mathbf{z}|}}{4\sqrt{\pi\kappa|\mathbf{x}-\mathbf{z}|}}e^{-i\kappa\mathbf{x}\cdot\hat{\mathbf{z}}}\{1+i\kappa(\frac{1}{2}\frac{|\mathbf{x}|^2}{|\mathbf{z}|}+|\mathbf{z}|R_2(\mathbf{x},\mathbf{z}))-\kappa^2(\frac{1}{2}\frac{|\mathbf{x}|^2}{|\mathbf{z}|}+|\mathbf{z}|R_2(\mathbf{x},\mathbf{z}))^2+...\} \\ &\quad\times\{1+O(\frac{1}{|\mathbf{x}-\mathbf{z}|})\} \end{aligned}$$

Clearly

$$\frac{1}{2}\frac{|\mathbf{x}|^2}{|\mathbf{z}|}+|\mathbf{z}|R_2(\mathbf{x},\mathbf{z})=O(\frac{1}{|\mathbf{z}|})$$

and so

$$\Phi(\mathbf{x},\mathbf{z})=\frac{(1+i)e^{i\kappa|\mathbf{z}|}}{4\sqrt{\pi\kappa|\mathbf{x}-\mathbf{z}|}}e^{-i\kappa\mathbf{x}\cdot\hat{\mathbf{z}}}\{1+O(\frac{1}{|\mathbf{z}|})\} \text{ as } |\mathbf{z}|\to\infty$$

Similarly, from (2.11) and (2.12) we see that for $|\mathbf{z}|$ sufficiently large

$$|\mathbf{x}-\mathbf{z}|^{-\frac{1}{2}}=|\mathbf{z}|^{-\frac{1}{2}}\{1+O(\frac{1}{|\mathbf{z}|})\} \tag{4.1}$$

from which

$$\Phi(\mathbf{x},\mathbf{z})=\frac{e^{i\pi/4}e^{i\kappa|\mathbf{z}|}}{\sqrt{8\pi\kappa|\mathbf{z}|}}e^{-i\kappa\mathbf{x}\cdot\hat{\mathbf{z}}}\{1+O(\frac{1}{|\mathbf{z}|})\} \text{ as } |\mathbf{z}|\to\infty \tag{4.2}$$

and so

$$\Phi(\mathbf{x},\mathbf{z})\sim\frac{e^{i\pi/4}e^{i\kappa|\mathbf{z}|}}{\sqrt{8\pi\kappa|\mathbf{z}|}}e^{-i\kappa\mathbf{x}\cdot\hat{\mathbf{z}}}=:\Lambda(\mathbf{x},\mathbf{z})$$

as $|\mathbf{z}| \to \infty$. This means that the field at fixed $\mathbf{x}$ corresponding to a point source at $\mathbf{z}$ tends asymptotically to the field due to plane waves travelling from the direction of the point source as $|\mathbf{z}| \to \infty$, but with a damping amplitude term, as seen illustrated in figures 8.2 to 8.4.

All radiating solutions $v(\mathbf{x})$ to the Helmholtz equation (and therefore solutions of the EADP) have asymptotic behaviour

$$v(\mathbf{x}) = \frac{e^{i\kappa|\mathbf{x}|}}{|\mathbf{x}|^{\frac{m-1}{2}}}\{v^\infty(\hat{\mathbf{x}}) + O(\frac{1}{|\mathbf{x}|})\} \qquad |\mathbf{x}| \to \infty$$

(see [3, p.21]) where $v^\infty(\hat{\mathbf{x}})$ is called the *far-field pattern*, defined for $\hat{\mathbf{x}} \in \Omega$. We see that the far-field pattern determines how the field varies with the direction in which we observe it, when observed for away.

In particular, $\Phi(\mathbf{x}, \mathbf{z})$ is a solution of the EADP, and so has this behaviour.

Theorem 3 *The fundamental solution to the Helmholtz equation for $m = 2$ has the asymptotic behaviour*

$$\Phi(\mathbf{x}, \mathbf{z}) = \frac{e^{i\kappa|\mathbf{x}|}}{\sqrt{|\mathbf{x}|}}\{\Phi_0^\infty(\hat{\mathbf{x}}, \mathbf{z}) + O(\frac{1}{|\mathbf{x}|})\} \qquad |\mathbf{x}| \to \infty$$

where the far-field pattern $\Phi_0^\infty(\hat{\mathbf{x}}, \mathbf{z})$ is given by

$$\Phi_0^\infty(\hat{\mathbf{x}}, \mathbf{z}) = \frac{e^{i\pi/4}}{\sqrt{8\pi\kappa}} e^{-i\kappa\mathbf{z}\cdot\hat{\mathbf{x}}} \tag{4.3}$$

Proof This follows immediately from (4.2) by interchanging the roles of $\mathbf{x}$ and $\mathbf{z}$ □

Since the field of scattered waves is a solution to the special case of the EADP, then for scattering of plane waves with direction $\hat{\mathbf{d}}$ we have

$$u^s(\mathbf{x}, \hat{\mathbf{d}}) = \frac{e^{i\kappa|\mathbf{x}|}}{|\mathbf{x}|^{\frac{m-1}{2}}}\{u^\infty(\hat{\mathbf{x}}, \hat{\mathbf{d}}) + O(\frac{1}{|\mathbf{x}|})\} \qquad |\mathbf{x}| \to \infty \tag{4.4}$$

for the far-field pattern $u^\infty(\hat{\mathbf{x}}, \hat{\mathbf{d}})$. Similarly, if we considered scattering of waves from a point source, with incident field given by $\Phi(\mathbf{x}, \mathbf{z})$, then the field of the scattered wave $\Phi^s(\mathbf{x}, \mathbf{z})$ has the behaviour

$$\Phi^s(\mathbf{x},\mathbf{z}) = \frac{e^{i\kappa|\mathbf{x}|}}{|\mathbf{x}|^{\frac{m-1}{2}}}\{\Phi^\infty(\hat{\mathbf{x}},\mathbf{z}) + O(\frac{1}{|\mathbf{x}|})\} \qquad |\mathbf{x}| \to \infty$$

with corresponding far-field pattern $\Phi^\infty(\mathbf{x},\mathbf{z})$.

We now turn our attention to finding the far-field pattern of (3.3). From (2.14) we have

$$H_1^{(1)}(x) = \sqrt{\frac{2}{\pi x}} e^{i\{x-\frac{3\pi}{4}\}}\{1 + O(\frac{1}{x})\} \qquad \text{as } |x| \to \infty$$

and so similarly to our derivation of (4.2) we obtain for fixed $\mathbf{z}$

$$H_1^{(1)}(\kappa|\mathbf{x}-\mathbf{z}|) = e^{-i\frac{3\pi}{4}}\sqrt{\frac{2}{\pi\kappa}}\frac{e^{i\kappa|\mathbf{x}|}}{\sqrt{|\mathbf{x}|}} e^{-i\kappa\mathbf{z}\cdot\hat{\mathbf{x}}}\{1 + O(\frac{1}{x})\} \qquad \text{as } |\mathbf{x}| \to \infty$$

and using (4.1) we can show that

$$\frac{\hat{\mathbf{n}}(\mathbf{z})\cdot(\mathbf{x}-\mathbf{z})}{|\mathbf{x}-\mathbf{z}|} = \hat{\mathbf{n}}(\mathbf{z})\cdot\hat{\mathbf{x}}\{1 + O(\frac{1}{|\mathbf{x}|})\} \qquad \text{as } |\mathbf{x}| \to \infty$$

Therefore

$$\frac{\partial\Phi(\mathbf{x},\mathbf{z})}{\partial\hat{\mathbf{n}}(\mathbf{z})} = \frac{e^{i\kappa|\mathbf{x}|}}{\sqrt{|\mathbf{x}|}}\{\frac{e^{-i\frac{\pi}{4}}\sqrt{\kappa}}{\sqrt{8\pi}}\hat{\mathbf{n}}(\mathbf{z})\cdot\hat{\mathbf{x}}e^{-i\kappa\mathbf{z}\cdot\hat{\mathbf{x}}} + O(\frac{1}{|\mathbf{x}|})\} \qquad \text{as } |\mathbf{x}| \to \infty$$

Recall the integral form (3.3) of the solution $u^s(\mathbf{x},\hat{\mathbf{d}})$ to the direct scattering problem. Substituting our expressions for the asymptotic behaviour of $\Phi(\mathbf{x},\mathbf{z})$ and its normal derivative as derived above, we obtain

$$u^s(\mathbf{x},\hat{\mathbf{d}}) = -\frac{e^{i\kappa|\mathbf{x}|}}{\sqrt{|\mathbf{x}|}}\frac{e^{i\frac{3\pi}{4}}}{\sqrt{8\pi\kappa}}\{\int_{\partial D} e^{-i\kappa\mathbf{z}\cdot\hat{\mathbf{x}}}\left(\kappa\hat{\mathbf{n}}(\mathbf{z})\cdot\hat{\mathbf{x}} + 1\right)\varphi(\mathbf{z})dS(\mathbf{z}) + O(\frac{1}{|\mathbf{x}|})\} \qquad \text{as } |\mathbf{x}| \to \infty$$

The corresponding far-field pattern is obtained by comparison with (4.4). Defining the operator $\mathcal{F}$ by

$$(\mathcal{F}\varphi)(\hat{\mathbf{x}}) := -\frac{e^{i\frac{3\pi}{4}}}{\sqrt{8\pi\kappa}}\int_{\partial D} e^{-i\kappa\mathbf{z}\cdot\hat{\mathbf{x}}}\left(\kappa\hat{\mathbf{n}}(\mathbf{z})\cdot\hat{\mathbf{x}} + 1\right)\varphi(\mathbf{z})dS(\mathbf{z})$$

we have that

$$u^\infty(\hat{\mathbf{x}},\hat{\mathbf{d}}) = (\mathcal{F}\varphi)(\hat{\mathbf{x}}) \tag{4.5}$$

where φ is given by

$$\varphi = -2(\mathcal{I} + \mathcal{K} - i\mathcal{S})^{-1}u^i(\mathbf{x},\hat{\mathbf{d}})|_{\partial D}$$

4.2 Reciprocity Relations

The point source method makes use of two theorems concerning the far-field patterns of scattered waves. The first concerns the far-field pattern for a scattered plane wave.

Theorem 4 *For scattering of plane waves in $\mathbb{R}^m$, $m = 1, 2$, the far-field pattern satisfies the relation*

$$u^\infty(\hat{\mathbf{x}}, \hat{\mathbf{d}}) = u^\infty(-\hat{\mathbf{d}}, -\hat{\mathbf{x}}) \qquad \hat{\mathbf{x}}, \hat{\mathbf{d}} \in \Omega \tag{4.6}$$

Proof See [9, p.42]. □

Theorem 5 *For scattering in $\mathbb{R}^m$ we have*

$$\Phi^\infty(\hat{\mathbf{x}}, \mathbf{z}) = \gamma_m u^s(\mathbf{z}, -\hat{\mathbf{x}}) \tag{4.7}$$

where

$$\gamma_2 = \frac{e^{i\pi/4}}{\sqrt{8\pi\kappa}}; \qquad \gamma_3 = \frac{1}{4\pi}$$

Proof See [9, p.43]. □

4.3 Potthast's Method

Potthast [7] uses the far-field pattern due to scattering of incident plane waves, to reconstruct the field close to the surface ∂D.

To implement his method we must make an assumption (or obtain *a priori* information) on the size and location of the domain D of the sound-soft scatterer. We denote $B_R(\mathbf{z}) = \{\mathbf{v} \in \mathbb{R}^m : |\mathbf{v} - \mathbf{z}| \leq R\}$ the ball in $\mathbb{R}^m$ of radius R centred on the point $\mathbf{z}$. We shall assume that $\bar{D} \subset B_R(\mathbf{0})$ for some known $R > 0$ (this is not quite the approach of Potthast [7], but serves the same purpose in that we have a bound on both the size and location of $\bar{D}$). See figure 4.1. This is not an unrealistic assumption in the practical application of solving the inverse problem: in medical applications we can at worst choose R to be the height of the patient.

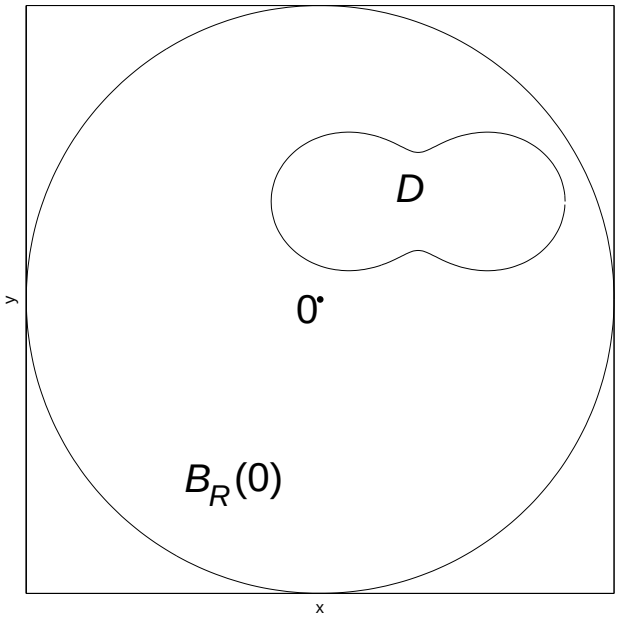

Figure 4.1: Assumptions on the location of the scatterer

For $\mathbf{x} \in S \subset \mathbb{R}^m$ and some density function $g \in L^2(\Omega)$, let $\mathcal{H}^i : L^2(\Omega) \to L^2(S)$ be the injective linear *Herglotz wave operator* defined by

$$(\mathcal{H}^i g)(\mathbf{x}) := \int_\Omega e^{i\kappa \mathbf{x}\cdot\hat{\mathbf{d}}} g(\hat{\mathbf{d}}) dS(\hat{\mathbf{d}}) \qquad \mathbf{x} \in S \tag{4.8}$$

We call $(\mathcal{H}^i g)$ the *Herglotz wave function*, which satisfies the Helmholtz equation.

Let $G_0 \subset \mathbb{R}^m \backslash \{\mathbf{0}\}$ be some open set bounded by $\partial G_0 \subset \mathbb{R}^m \backslash \{\mathbf{0}\}$ (with closure $\bar{G}_0 = G_0 \cup \partial G_0$), for which there exist points $\mathbf{z} \in \mathbb{R}^m \backslash \bar{D}$ and corresponding rotations $M(\mathbf{z})$ such $\bar{D} \subset G(\mathbf{z}) = M(\mathbf{z})G_0 + \mathbf{z}$, i.e. there exist points to which we can rotate and translate G_0 such that it contains $\bar{D}$ (hence the need for a priori information about the scatterer). $G(\mathbf{z})$ will be our *domain of approximation*.

We assume that G_0 is such that $\mathcal{H}^i$ has dense range in $L^2(\partial G_0)$. By definition, this means that given $\epsilon > 0$ and $f \in L^2(\partial G_0)$, then there exists $g \in L^2(\Omega)$ such that

$$\|f - (\mathcal{H}^i g)\|_{L^2(\partial G_0)} \leq \epsilon$$

and in particular since $\Phi(\mathbf{x},\mathbf{0}) \in L^2(\partial G_0)$, for a given $\epsilon > 0$ we can find $g_0 \in L^2(\partial G_0)$ such that

$$\|\Phi(\cdot,\mathbf{0}) - (\mathcal{H}^i g_0)\|_{L^2(\partial G_0)} \leq \epsilon$$

Interior Dirichlet Problem (IDP) *Find $v \in C^2(\Pi) \cap C(\bar{\Pi})$ such that for $h \in C(\partial\Pi)$*

$$\begin{aligned} (\Delta + \kappa^2)v(\mathbf{x}) &= 0 \qquad \mathbf{x} \in \Pi \\ v(\mathbf{x}) &= h(\mathbf{x}) \qquad \mathbf{x} \in \partial\Pi \end{aligned}$$

Clearly, for $\Pi = G_0$ then both $\Phi(\cdot,\mathbf{0})$ and $(\mathcal{H}^i g_0)$ satisfy the IDP for $h = \Phi(\cdot,\mathbf{0})|_{\partial G_0}$ and $h = (\mathcal{H}^i g_0)|_{\partial G_0}$ respectively, and therefore so does $\Phi(\cdot,\mathbf{0}) - (\mathcal{H}^i g_0)$ with $h = (\Phi(\cdot,\mathbf{0}) - \mathcal{H}^i g_0)|_{\partial G_0}$. Potthast [9, p.125] claims that on all compact subsets of Π solutions to this problem depend continuously on the boundary values in $L^2(\partial\Pi)$, therefore for some $\bar{G}_{sub} \subset G_0$ where $\bar{G}_{sub}$ is closed, then

$$\|\Phi(.,\mathbf{0}) - \mathcal{H}^i g_0\|_{C(\bar{G}_{sub})} \leq \tau \|\Phi(.,\mathbf{0}) - \mathcal{H}^i g_0\|_{L^2(\partial G_0)} \leq \tau\epsilon \tag{4.9}$$

for some $\tau = \tau(G_0,\kappa) > 0$ (i.e. the constant depends on Π and κ in the IDP).

Now, we perform a translation by vector $\mathbf{z}$ and rotation by orthogonal matrix $M(\mathbf{z})$ of both the domain of approximation and the wave function. So $G_0 \mapsto G(\mathbf{z}) = M(\mathbf{z})G_0 + \mathbf{z}$, and similarly $G_{sub} \mapsto \bar{G}_{sub}(\mathbf{z}) := M(\mathbf{z})\bar{G}_{sub} + \mathbf{z}$. $(\mathcal{H}^i g_0)(\mathbf{x})$ maps to

$$\begin{aligned} (\mathcal{H}^i g_0)(M^{-1}(\mathbf{x}-\mathbf{z})) &= \int_\Omega e^{i\kappa M^{-1}(\mathbf{x}-\mathbf{z})\cdot\hat{\mathbf{d}}} g_0(\hat{\mathbf{d}}) dS(\hat{\mathbf{d}}) \\ &= \int_\Omega e^{i\kappa M^{-1}\mathbf{x}\cdot\hat{\mathbf{d}}} e^{-i\kappa M^{-1}\mathbf{z}\cdot\hat{\mathbf{d}}} g_0(\hat{\mathbf{d}}) dS(\hat{\mathbf{d}}) \\ &= \int_\Omega e^{i\kappa (M^T\mathbf{x})\cdot\hat{\mathbf{d}}} e^{-i\kappa (M^T\mathbf{z})\cdot\hat{\mathbf{d}}} g_0(\hat{\mathbf{d}}) dS(\hat{\mathbf{d}}) \text{ since } M \text{ is orthogonal} \\ &= \int_\Omega e^{i\kappa\mathbf{x}\cdot M\hat{\mathbf{d}}} e^{-i\kappa\mathbf{z}\cdot M\hat{\mathbf{d}}} g_0(\hat{\mathbf{d}}) dS(\hat{\mathbf{d}}) \\ &= \int_\Omega e^{i\kappa\mathbf{x}\cdot\hat{\mathbf{t}}} e^{-i\kappa\mathbf{z}\cdot\hat{\mathbf{t}}} g_0(M^{-1}\hat{\mathbf{t}}) dS(\hat{\mathbf{t}}) \quad \text{for } \hat{\mathbf{t}} := M\hat{\mathbf{d}} \in \Omega \\ &= \int_\Omega u^i(\mathbf{x},\hat{\mathbf{t}}) g_{\mathbf{z}}(\hat{\mathbf{t}}) dS(\hat{\mathbf{t}}) \end{aligned}$$

$$=: \quad (\mathcal{H}^i g_{\mathbf{z}})(\mathbf{x})$$

where $g_{\mathbf{z}}(\hat{\mathbf{t}}) := e^{-i\kappa \mathbf{z}\cdot\hat{\mathbf{t}}} g_0(M^{-1}\hat{\mathbf{t}})$. Then, under this mapping we have that

$$\|\Phi(\mathbf{x},\mathbf{z}) - \mathcal{H}^i g_{\mathbf{z}}\|_{C(\bar{G}_{sub}(\mathbf{z}))} \leq \tau\epsilon$$

and so provided that $\bar{G}_{sub}$ is large enough that $D \subset \bar{G}_{sub}(\mathbf{z})$

$$\|\Phi(\mathbf{x},\mathbf{z}) - \mathcal{H}^i g_{\mathbf{z}}\|_{C(D)} \leq \tau\epsilon$$

The operator $\mathcal{F}$ mapping the incident field to its corresponding far-field pattern is bounded [9, p.173], and so there exists $c > 0$ such that

$$\begin{aligned} \|\Phi^\infty(\hat{\mathbf{x}},\mathbf{z}) - (\mathcal{H}^\infty g_{\mathbf{z}})(\hat{\mathbf{x}})\|_{C(\Omega)} &\leq c\|\Phi(\mathbf{x},\mathbf{z}) - (\mathcal{H}^i g_{\mathbf{z}})(\mathbf{x})\|_{C(D)} \\ &\leq c\tau\epsilon \end{aligned}$$

where

$$(\mathcal{H}^\infty g_{\mathbf{z}})(\hat{\mathbf{x}}) := \int_\Omega u^\infty(\hat{\mathbf{x}},\hat{\mathbf{d}}) g_{\mathbf{z}}(\hat{\mathbf{d}}) dS(\hat{\mathbf{d}})$$

So, using Theorem 4 we have that, for a given $\hat{\mathbf{t}} \in \Omega$

$$\|\Phi^\infty(-\hat{\mathbf{t}},\mathbf{z}) - \int_\Omega u^\infty(-\hat{\mathbf{d}},\hat{\mathbf{t}}) g_{\mathbf{z}}(\hat{\mathbf{d}}) dS(\hat{\mathbf{d}}))\|_{C(\Omega)} \leq c\tau\epsilon$$

Then by application of Theorem 5

$$\|u^s(\mathbf{z},\hat{\mathbf{t}}) - \frac{1}{\gamma_m}\int_\Omega u^\infty(-\hat{\mathbf{d}},\hat{\mathbf{t}}) g_{\mathbf{z}}(\hat{\mathbf{d}}) dS(\hat{\mathbf{d}}))\|_{C(\Omega)} \leq \frac{c\tau\epsilon}{|\gamma_m|} \tag{4.10}$$

To summarise, the point source method offers a way to approximate the scattered field at a point $\mathbf{z} \in \mathbb{R}^m \backslash \bar{D}$ by way of obtaining the far-field pattern. It breaks down the inverse problem into two parts: the first is to obtain our function g_0 (given a suitable domain of approximation G_0); the second is to successfully implement (4.10) to reconstruct the field around the scatterer. The smaller we can make ϵ in the first part, the more accurate our approximation will be in the second.

Chapter 5

Obtaining a Suitable g_0

So far we have had to assume that we can find some $G_0 \subset \mathbb{R}^m \backslash \{\mathbf{0}\}$ such that $\mathcal{H}^i$ has dense range in $L^2(\partial G_0)$. This is shown to be possible in the following theorem.

Theorem 6 *It is possible to choose a domain $G_0 \subset \mathbb{R}^m \backslash \{\mathbf{0}\}$ with boundary ∂G_0 of class C^2 such that the homogeneous interior Dirichlet problem*

$$\begin{aligned} (\Delta + \kappa^2)v(\mathbf{x}) = 0 \quad & \mathbf{x} \in G_0 \\ v(\mathbf{x}) = 0 \quad & \mathbf{x} \in \partial G_0 \end{aligned}$$

has only the trivial solution $v \equiv 0$. In this case the operator $\mathcal{H}^i$ has dense range in $L^2(\partial G_0)$

Proof See [9, p.123] $\square$

Let $v(\mathbf{x}) := \Phi(\mathbf{x}, \mathbf{0}) - (\mathcal{H}^i g)(\mathbf{x})$ defined for all $\mathbf{x} \in \mathbb{R}^m \backslash \{\mathbf{0}\}$, and G_0 be such that theorem 6 holds. If we arrange for v to be zero on the boundary ∂G_0 (through our choice of g), then by the theorem $v = 0$ on G_0 also. However, referring to Colton and Kress [4, p.72] we see that if for any twice continuously differentiable function w solving the Helmholtz equation on some domain Π, we have that $w(\mathbf{x}) = 0$ on any neighbourhood of some $\mathbf{x}_0 \in \Pi$, then $w \equiv 0$ everywhere in Π (which we refer to as *unique continuation for the Helmholtz equation*). As a consequence of this, $v = 0$ on G_0 implies that $v \equiv 0$ on the whole of $\mathbb{R}^m \backslash \{\mathbf{0}\}$.

However, this leads us to a contradiction since $\Phi(\mathbf{x}, \mathbf{0}) \to \infty$ as $\mathbf{x} \to \mathbf{0}$ (and so v cannot be zero at all points except $\mathbf{0}$). Therefore, we conclude that there is no function g that solves the first kind integral equation

$$\Phi(\mathbf{x}, \mathbf{0}) = \int_\Omega e^{i\kappa \mathbf{x} \cdot \hat{\mathbf{d}}} g(\hat{\mathbf{d}}) dS(\hat{\mathbf{d}}) \qquad \mathbf{x} \in \partial G_0 \tag{5.1}$$

Hence Potthast's approach, in which we show that we can find some g_0 for which the integral equation is satisfied approximately to arbitrary accuracy. However, we are still left with the problem of how to obtain this function.

5.1 Tikhonov Regularisation

The problem $Ax = y$ is said to be well-posed if

- There exists a solution
- The solution x is unique
- x depends continuously upon y (and so is stable with respect to perturbations in y)

If at least one of these criteria are not met, then the problem is said to be ill-posed.

Clearly (5.1) is ill-posed, since we do not have existence of a solution. Traditionally ill-posed problems have been ignored, though techniques have been developed to deal with such problems, in particular that of *Tikhonov regularisation*.

Let X and Y be Hilbert spaces with norm $\|.\|$, and $A : X \to Y$ be an injective bounded linear operator. Then a *regularisation scheme* for A is a family of bounded linear operators $R_\alpha : Y \to X$, $\alpha > 0$ such that

$$\lim_{\alpha \to 0} R_\alpha y = x \qquad \text{for all } x \in X$$

We define the *Tikhonov functional* by

$$J_\alpha(x) := \|Ax - y\|^2 + \alpha \|x\|^2$$

For $\alpha > 0$, J_α has a unique minimum at x_α which uniquely solves the *perturbed normal equation*

$$\begin{aligned} \alpha x_\alpha + A^* A x_\alpha &= A^* y \\ \text{i.e. } (\alpha I + A^* A) x_\alpha &= A^* y \end{aligned}$$

where I is the identity operator and A^* is the adjoint of A. Furthermore, x_α depends continuously on y [3, p.98], and so the method is stable. Then, for $\alpha > 0$ we can choose as our regularisation scheme

$$R_\alpha := (\alpha I + A^*A)^{-1}A^* : Y \to X$$

since for $\alpha > 0$, $(\alpha I + A^*A)$ is bijective [3, p.97], and so we can compute

$$x_\alpha = (\alpha I + A^*A)^{-1}A^*y$$

which is the unique solution of the perturbed normal equation.

5.2 Application of Tikhonov Regularisation

We approach the problem of finding a suitable g_0 by employing Tikhonov regularisation to solve (5.1). The adjoint of $(\mathcal{H}^i g)$ is given by

$$(\mathcal{H}^{i*}g)(\mathbf{x}) = \int_\Omega e^{-i\kappa\mathbf{x}\cdot\hat{\mathbf{d}}} g(\hat{\mathbf{d}}) dS(\hat{\mathbf{d}})$$

Then, since L^2 is a Hilbert space, we can apply the technique of Tikhonov regularisation to $\mathcal{H}^i$ and $\Phi(\mathbf{x}, \mathbf{0})$. Letting R_α $(\alpha > 0)$ be given by

$$R_\alpha = (\alpha\mathcal{I} + \mathcal{H}^{i*}\mathcal{H}^i)^{-1}\mathcal{H}^{i*}$$

we can then calculate $g_0^\alpha = R_\alpha\Phi(\mathbf{x}, \mathbf{0})$.

Chapter 6

Implementation of Point Source Method

We can say something about the success of Potthast's method by applying it to our peanut shaped sound-soft scatterer, with known location, for scattering of a plane wave with known direction of incidence $\hat{\mathbf{t}}$. We aim to reconstruct the the total field on $B_3(\mathbf{0})$, which is known to contain our $\bar{D}$.

We discretise the boundary ∂G_0 by the set of points $\{\mathbf{x}_r\}_{r=1}^R$, and $B_3(\mathbf{0})$ by the set $\{\mathbf{z}_t\}_{t=1}^T$. We suppose that ∂D can be parameterised by some 2π periodic function $\mathbf{q}(\phi)$ for $\phi \in [0, 2\pi)$ (as in section 3.3), and so discretise ∂D by the set $(\mathbf{q}(\phi_j))_{j=1}^J$ for $\phi_j = j2\pi/J$.

Discretise Ω by the ordered set $\left(\hat{\mathbf{d}}_n = (\cos((n-1)\Delta\theta), \sin((n-1)\Delta\theta))^T\right)_{n=1}^N$ where $\Delta\theta = 2\pi/N$ and N is even, and let $h^\alpha(\hat{\mathbf{d}}_i)$ be our numerical solution for $g_0^\alpha(\hat{\mathbf{d}}_i)$. To implement the point source method we must be able to use the set $\left(h^\alpha(\hat{\mathbf{d}}_n)\right)_{n=1}^N$ to obtain the set $\left(h^\alpha(M^{-1}(\mathbf{z}_t)\hat{\mathbf{d}}_n)\right)_{n=1}^N$ for each $\mathbf{z}_t$ where $M(\mathbf{z}_t)$ is as before (i.e. a rotation such that $\bar{D}$ is contained in the rotated and translated domain of approximation).

Now let us use the rule that each rotation $M(\mathbf{z}_t)$ which rotates G_0 by an angle θ_t will be such that $\theta_t = \tau_t\Delta\theta$, for integral $\tau_t \geq 0$, i.e.

$$M(\mathbf{z}_t) = \begin{pmatrix} \cos(\tau_t\Delta\theta) & \sin(\tau_t\Delta\theta) \\ -\sin(\tau_t\Delta\theta) & \cos(\tau_t\Delta\theta) \end{pmatrix} \qquad \tau_t \in \mathbb{N}\backslash\{0\}$$

Then the mapping from $\left(h^\alpha(\hat{\mathbf{d}}_n)\right)_{n=1}^N$ to $\left(h^\alpha(M^{-1}(\mathbf{z}_t)\hat{\mathbf{d}}_n)\right)_{n=1}^N$ is a simple permutation $\wp(\tau_t)$

where for $\tau_t > 0$

$$\begin{aligned}\wp(\tau_t)(h^\alpha(\hat{\mathbf{d}}_1), ..., h^\alpha(\hat{\mathbf{d}}_N)) &\mapsto (h^\alpha(\hat{\mathbf{d}}_{\tau_t+1}), ..., h^\alpha(\hat{\mathbf{d}}_N), h^\alpha(\hat{\mathbf{d}}_1), ..., h^\alpha(\hat{\mathbf{d}}_{\tau_t})) \\ &=: (f^\alpha_{t,1}, ..., f^\alpha_{t,N})\end{aligned}$$

and $\wp(\tau_t)$ is the identity permutation for $\tau_t = 0$.

We must obtain the far-field pattern in each direction $-\hat{\mathbf{d}}_n$. Let $w^\infty(-\hat{\mathbf{d}}_n, \hat{\mathbf{t}})$ be our numerical solution to $u^\infty(-\hat{\mathbf{d}}_n, \hat{\mathbf{t}})$. Then by applying the trapezium rule to our expression for $\mathcal{F}$ we have

$$w^\infty(-\hat{\mathbf{d}}_n, \hat{\mathbf{t}}) = -\frac{e^{i\frac{3\pi}{4}}}{\sqrt{8\pi\kappa}} \frac{2\pi}{J} \sum_{j=1}^{J} e^{i\kappa\mathbf{q}(\phi_j)\cdot\hat{\mathbf{d}}_n}(1 - \kappa\mathbf{q}(\phi_j)\cdot\hat{\mathbf{d}}_n)\varphi(\mathbf{q}(\phi_j)|\mathbf{q}'(\phi_j)|$$

where $\varphi(\mathbf{q}(\phi_j))$ is obtained as in section (3.3).

To obtain our numerical solution $h^\alpha(\hat{\mathbf{d}}_i)$, let $\vec{h}^\alpha = (h^\alpha(\hat{\mathbf{d}}_1), ..., h^\alpha(\hat{\mathbf{d}}_N))^T$, and define the $R \times N$ matrix H by

$$H(r, n) = \Delta\theta e^{i\kappa\mathbf{x}_r\cdot\hat{\mathbf{d}}_n}$$

We then calculate

$$\vec{h^\alpha} = (\alpha I + H^*H)^{-1}H^*\vec{\Phi}_0 \tag{6.1}$$

where α is small, I is the $N \times N$ identity matrix, H^* is the conjugate transpose of H, and $\vec{\Phi}_0 := (\Phi(\mathbf{x}_1, \mathbf{0}), ..., \Phi(\mathbf{x}_R, \mathbf{0}))^T$

We wish to reconstruct the field at each $\mathbf{z}_t$ using the point source method. By applying the trapezium rule to (4.10) we have

$$w^s(\mathbf{z}_t) = \frac{1}{\gamma_2}\Delta\theta \sum_{n=1}^{N} w^\infty(-\hat{\mathbf{d}}_n, \hat{\mathbf{t}})e^{-i\kappa\mathbf{z}_t\cdot\hat{\mathbf{d}}_n} f^\alpha_{t,n}$$

6.1 Choice of G_0

We must make a choice as to the geometry of G_0. In [7] Potthast assumes an *exterior cone condition*. Let $\mathcal{C}_{\mathbf{x},\hat{\mathbf{p}},\beta}$ denote the set $\{\mathbf{y} \in \mathbb{R}^m : (\mathbf{y}-\mathbf{x}) \cdot \hat{\mathbf{p}} \geq \cos\beta\}$, which is a cone with vertex $\mathbf{x}$, direction $\hat{\mathbf{p}}$ and opening angle β (see figure 6.1). The exterior cone condition is that, for a known $\beta > 0$, then for all $\mathbf{x} \in \mathbb{R}^m \backslash D$ there exists a cone $\mathcal{C}_{\mathbf{x},\hat{\mathbf{p}},\beta}$ for some direction $\hat{\mathbf{p}} = \hat{\mathbf{p}}(\mathbf{x}) \in \Omega$ such that $D \cap \mathcal{C}_{\mathbf{x},\hat{\mathbf{p}},\beta} = \emptyset$.

We make use of this assumption, by defining G_0 by

$$G_0 := B_R(-\varepsilon\mathbf{i}) \backslash \mathcal{C}_{-\varepsilon\mathbf{i},\mathbf{i},\beta} \subset \mathbb{R}^m$$

where β is as above, ε is small, and R sufficiently large enough for our requirements (see figure 6.2). For our particular hippopede scatterer, $\bar{D}$ can be bounded by the ball $B_{3/2}(\mathbf{0})$, and we can find some β to give us our exterior cone condition. To reconstruct the field about the scatterer on the disc $B_3(\mathbf{0}) \backslash \bar{D}$, we can choose G_0 to be

$$G_0 = B_{9/2}(-\varepsilon\mathbf{i}) \backslash \mathcal{C}_{-\varepsilon\mathbf{i},\mathbf{i},\beta}$$

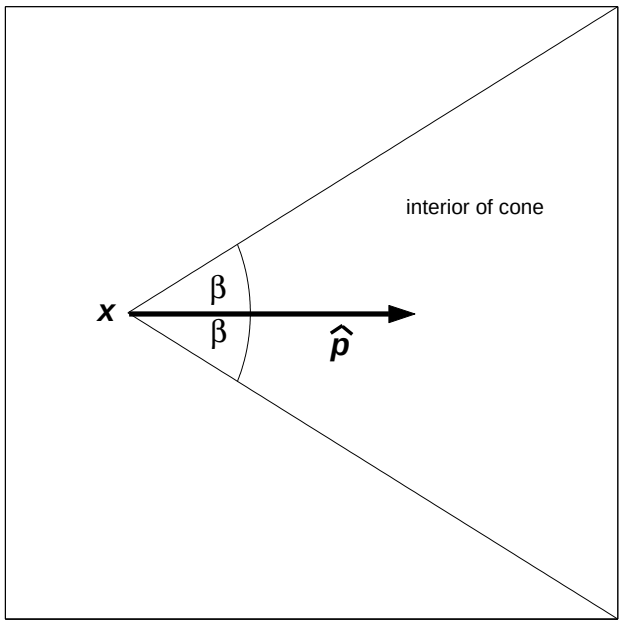

Figure 6.1: The cone $\mathcal{C}_{\mathbf{x},\hat{\mathbf{p}},\beta}$

The benefits of this shape for G_0 are that, provided $\mathcal{H}^i$ has dense range in $L^2(\partial G_0)$ then we can hope to reconstruct the field reliably at points very close to the surface of the scatterer (provided we have the exterior cone condition).

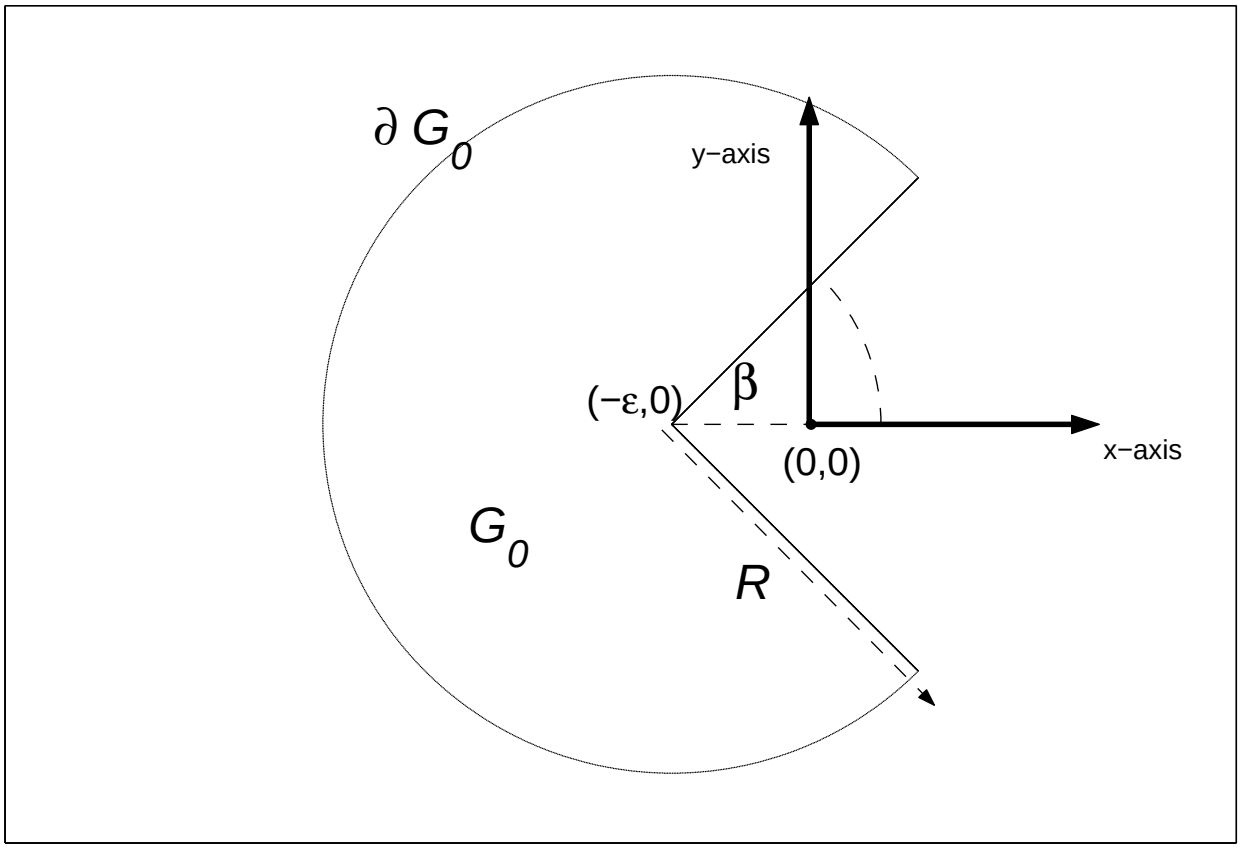

Figure 6.2: The domain of approximation G_0 given by $B_R(-\epsilon\mathbf{i})\backslash\mathcal{C}_{-\epsilon\mathbf{i},\mathbf{i},\beta}$

Since it is not of class C^2 we know that Theorem 6 cannot apply. However, the theorem does not rule out the range of $\mathcal{H}^i$ being dense in $L^2(\partial G_0)$ for this G_0. Nor does it suggest how we might construct such a domain. Nevertheless, we will illustrate that G_0 as defined above can successfully be used as the domain of approximation.

Theorem 7 *Consider the problem $Ax = y$ for the operator $A : X \to Y$ where X and Y are Hilbert spaces, and A is injective with dense range. If $y \in Y$, $y \neq 0$, $\alpha > 0$, and x^α is the unique solution of the perturbed normal equation, then x^α depends continuously on α. Furthermore*

- *The mapping $\alpha \to \|x^\alpha\|$ is strictly monotonically decreasing and $\lim_{\alpha\to\infty} = 0$*
- *The mapping $\alpha \to \|Ax^\alpha - y\|$ is strictly monotonically increasing and $\lim_{\alpha\to 0} \|Ax^\alpha - y\| = 0$*

Proof See [5, p.22] □

In our case $H : \mathbb{C}^N \to \mathbb{C}^R$, where N is the number of directions discretising Ω and R is the number of points discretising G_0, and the appropriate norm to look for convergence in is the ℓ^2-norm, $\|\cdot\|_2$ where

$$\|\mathbf{v}\|_2 = \sqrt{\sum_{r=1}^{R} |v_i|^2} \qquad \mathbf{v} = (v_1, ..., v_R)^T \in \mathbb{C}^R$$

Clearly, since $\vec{\Phi}_0 \neq \mathbf{0}$ then theorem 7 should apply if our particular G_0 is such that the range of H is dense in $\ell^2(\partial G_0)$. Figure 6.3 illustrates the required relationship ($\|\vec{h}^\alpha\|_2$ is strictly monotonically decreasing with increasing α), as well as convergence of $\|\vec{h}^\alpha\|_2$ as $\alpha \to \infty$.

Similarly $\|\vec{\Phi}_0 - H\vec{h}^\alpha\|_2$ can be shown to be strictly monotonically increasing with increasing α, and it can be seen in figure 6.4 that the greatest rate of increase occurs at $\alpha = 1$, whilst $\|\vec{\Phi}_0 - H\vec{h}^\alpha\|_2$ tends to zero as $\alpha \to 0$, as expected.

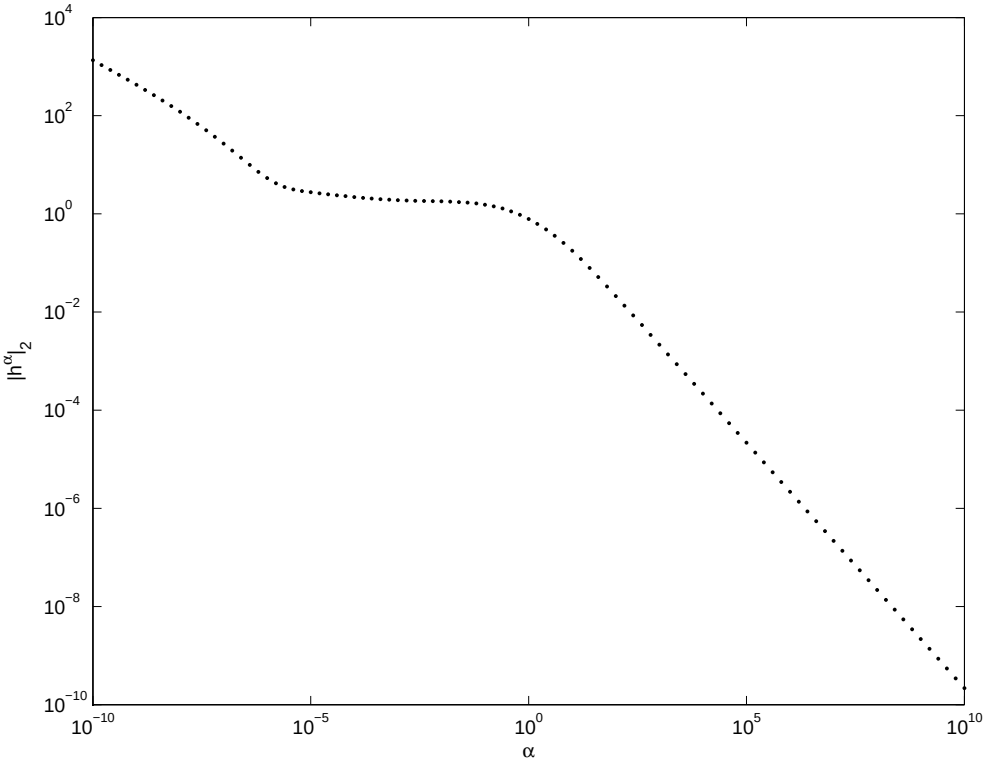

Figure 6.3: Convergence of $\|\vec{h}^\alpha\|_2$ as $\alpha \to \infty$ ($\log_{10}$ vs. $\log_{10}$ scale)

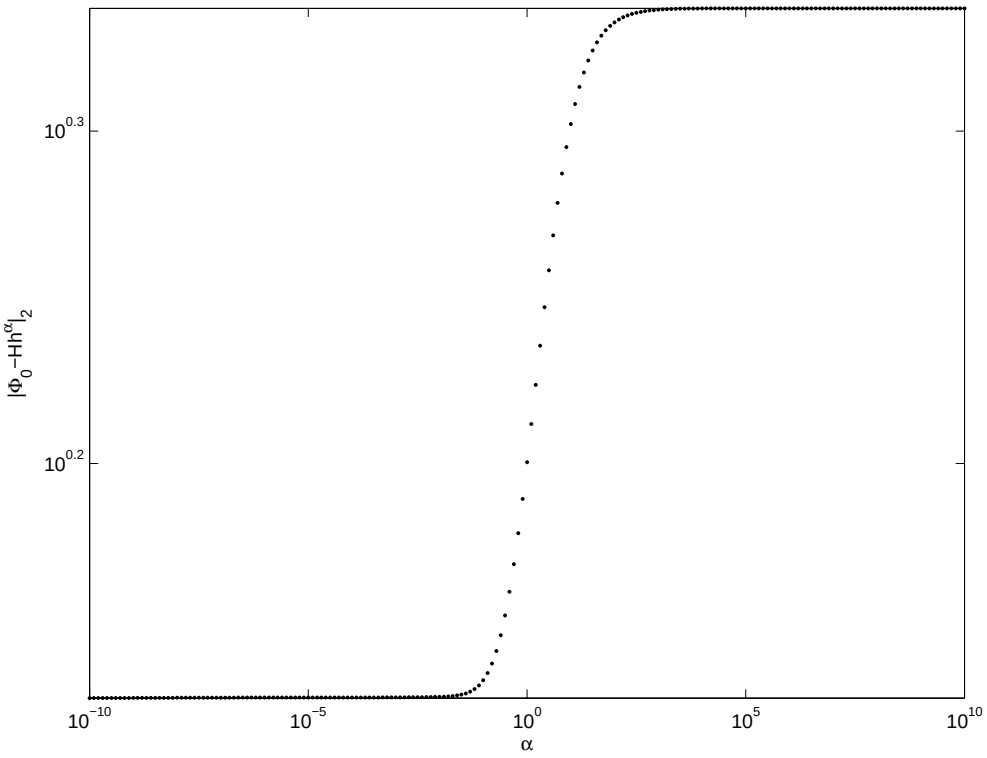

Figure 6.4: Convergence of $\|\vec{\Phi}_0 - H\vec{h}^\alpha\|_2$ as $\alpha \to 0$ ($\log_{10}$ vs. $\log_{10}$ scale)

Theorem 8 *Consider the operator $A : X \to Y$ where X and Y are Hilbert spaces, and A is injective with dense range. Then for x^α our result from applying the technique of Tikhonov regularisation to the problem $Ax = y$ for $x \in X$ and $y \in Y$*

- *y is in the range of $A \implies \lim_{\alpha\to 0}$ exists, and $x^\alpha \to x$*
- *y is not in the range of $A \implies \|x^\alpha\| \to \infty$ as $\alpha \to 0$*

Proof See [5, p.24]. □

We have proved that if ∂G_0 is such that the Helmholtz equation with zero Dirichlet boundary conditions has only the trivial solution, then there is no solution to (5.1) and therefore we expect $\|\vec{h}^\alpha\|_2$ to grow unboundedly as $\alpha \to 0$. However, instability occurs as α approaches 10^{-15}, and so it is not possible to illustrate unbounded growth or convergence as α becomes very small, in either case. This is because as α approaches the machine accuracy, the perturbed normal equation is lost as $\alpha I \approx 0$, and so MATLAB attempts to solve

$$H^* H\vec{h}^\alpha = H^*\vec{\Phi}_0$$

which is ill-posed if $H\vec{h}^{\alpha} = \vec{\Phi}_0$ is ill-posed. Therefore as $\alpha \to 0$ the condition number of $(\alpha I + H^*H)$ tends to zero and we approach a singular system. Though accuracy is increased by decreasing α, we are restricted by practical computing limitations.

Of interest to us, is how the choice of opening angle β affects the accuracy of our solution for a given α, as we have already observed in (4.9) that τ (a constant involved in the error estimate of our approximation) depends upon the geometry of G_0. Clearly (see figure 6.2) the limiting case for ∂G_0 as $\beta \to 0$ is a set of points including the origin, and therefore we cannot arrange for $\Phi(\mathbf{x}, \mathbf{0})$ and $(\mathcal{H}^i g_0)(\mathbf{x})$ to agree everywhere on ∂G_0. Therefore, since $\beta \in (0, \pi/2)$ we would expect closest agreement in our approximation for a G_0 with $\beta = \pi/2$.

Figure 6.5 is a graph of relative error $\|\vec{\Phi}_0 - H\vec{h}^{\alpha}\|/\|\vec{\Phi}_0\|$ for $\alpha = 10^{-10}$, and all such graphs for $\alpha < 1$ have the characteristics shown: namely, a global minimum at $\beta = \pi/2$ which rapidly increases before levelling off, suggesting that where possible we should use large cone opening angles. In the presence of an exterior cone condition, the success of the point source method is dependent upon this condition not being violated, and therefore there must be some compromise in the choice of β.

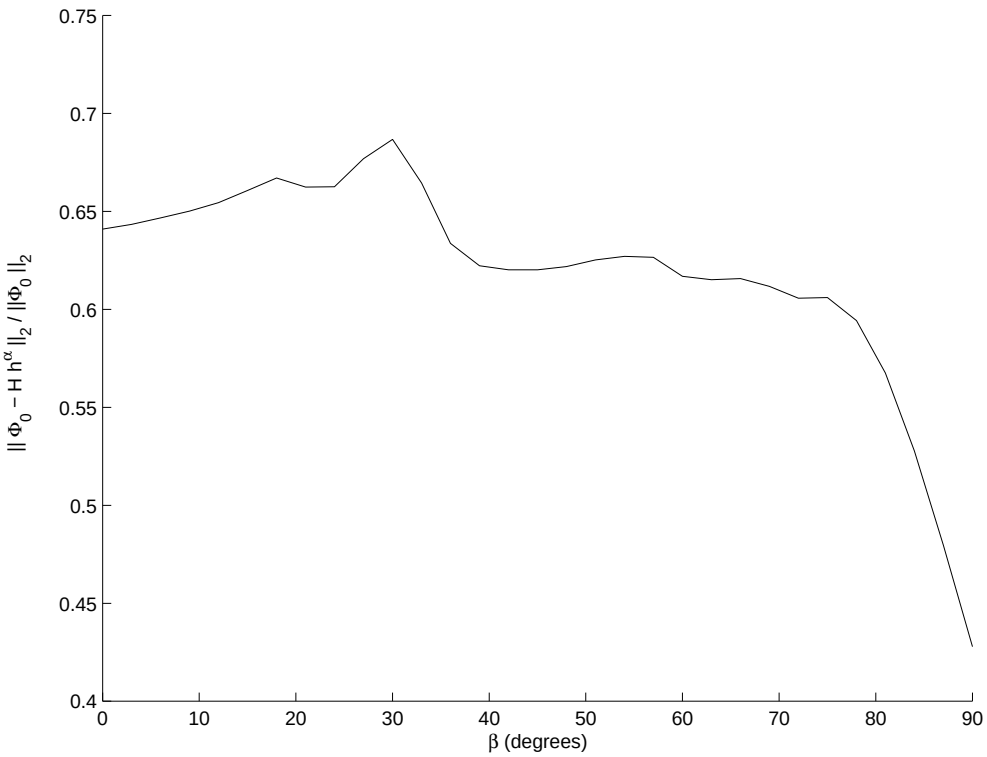

Figure 6.5: $\|\vec{\Phi}_0 - H\vec{h}^{\alpha}\|_2/\|\vec{\Phi}_0\|_2$ vs β (degrees) (with $\alpha = 10^{-10}$)

6.2 Object Location

So far we have discussed how to reconstruct the scattered field close to a scatterer, from measurements of its far-field pattern, in order to demonstrate the use of the reciprocity theorems and the effectiveness of Potthast's method. Of course, we would like to be able apply this method to locating an unknown sound-soft scatterer.

Theorem 9 *Recall the definitions of* $\Phi^\infty(\hat{\mathbf{x}}, \mathbf{z})$ *and* $\Phi_0^\infty(\hat{\mathbf{x}}, \mathbf{z})$. *Then for* $D \subset \mathbb{R}^3$ *the interior of a sound-soft scatterer, we have*

$$\begin{aligned} \mathbf{z} \in D &\implies \Phi^\infty(., \mathbf{z}) + \Phi_0^\infty(., \mathbf{z}) = 0 \\ \mathbf{z} \notin \bar{D} &\implies \Phi^\infty(., \mathbf{z}) + \Phi_0^\infty(., \mathbf{z}) \neq 0 \end{aligned}$$

Furthermore, $\Phi^\infty(., \mathbf{z}) \in C(\Omega)$ *depends continuously on* $\mathbf{z} \in \mathbb{R}^m$.

Proof See [7] □

Given that

$$\begin{aligned} \Phi^\infty(-\hat{\mathbf{t}}, \mathbf{z}) + \Phi_0^\infty(-\hat{\mathbf{t}}, \mathbf{z}) &= \gamma_2 u^s(\mathbf{z}, \hat{\mathbf{t}}) + \gamma_2 u^i(\mathbf{z}, \hat{\mathbf{t}}) \quad \text{using theorem 3 and theorem 4} \\ &= \gamma_2 u^t(\mathbf{z}, \hat{\mathbf{t}}) \end{aligned}$$

then by the theorem the total field at $\mathbf{z}$ will tend smoothly to zero as $\mathbf{z}$ approaches the scatterer. Therefore, defining the function

$$\delta(\mathbf{z}) := |u^t(\mathbf{z}, \hat{\mathbf{t}})|$$

we can locate the boundary ∂D by searching for the zeros of $\delta(\mathbf{z})$. Of course, we only have an approximation to the total field, which we denote as

$$\delta^\alpha(\mathbf{z}) := |e^{i\kappa \mathbf{z}\cdot\hat{\mathbf{t}}} + e^{-i\pi/4}\sqrt{8\pi\kappa} \int_\Omega u^\infty(-\hat{\mathbf{d}}, \mathbf{t}) g_{\mathbf{z}}(\hat{\mathbf{d}}) dS(\hat{\mathbf{d}})|$$

for Tikhonov regularisation parameter $\alpha > 0$, and so we can attempt to locate ∂D by finding where the minima of $\delta^\alpha(\mathbf{z})$ occur. Of course, only having an approximation available we lose

the property of uniqueness, in that there may be points for which δ^α is small, which are not in ∂D.

Algorithm for the point source method

- Identify $B_R(\mathbf{0})$ *known* to contain $\bar{D}$ (in our case we will use $R = 3$)
- Decompose $B_R(\mathbf{0})$ into disjoint domains $B_R^1(\mathbf{0})$,...,$B_R^N(\mathbf{0})$ such that $B_R(\mathbf{0}) = \bigcup_{i=1}^N B_R^i(\mathbf{0})$
- Choose an opening angle for G_0
- Choose a direction $\hat{\mathbf{p}}_i$ for each $B_R^i(\mathbf{0})$ giving the orientation (i.e. cone direction/rotation matrix) for $G(M, \mathbf{z})$ when $\mathbf{z} \in B_R^i(\mathbf{0})$
- In this way compute $\delta^\alpha(\mathbf{z})$ for each $\mathbf{z} \in B_R(\mathbf{0})$
- Plot the points for which $\delta(\mathbf{z})$ is small

With our particular shaped scatterer, and for the unit vectors $\mathbf{i} = (1, 0)^T$ and $\mathbf{j} = (0, 1)^T$, we can choose rotation angles θ_t by

$$\begin{aligned}
&\mathbf{z} \cdot \mathbf{i} > 1/\sqrt{2} && \implies \theta_t = 0 \\
&\mathbf{z} \cdot \mathbf{i} < -1/\sqrt{2} && \implies \theta_t = \pi \\
&|\mathbf{z} \cdot \mathbf{i}| \leq 1/\sqrt{2} \text{ and } \mathbf{z} \cdot \mathbf{j} > 0 && \implies \theta_t = \pi/2 \\
&|\mathbf{z} \cdot \mathbf{i}| \leq 1/\sqrt{2} \text{ and } \mathbf{z} \cdot \mathbf{j} \leq 0 && \implies \theta_t = 3\pi/2
\end{aligned}$$

In figure 8.5 we plot $\exp\{-10\delta^\alpha(\mathbf{z})\}$ for $\mathbf{z} \in B_3(\mathbf{0})$ (and so $\delta^\alpha(\mathbf{z})$ is smallest in red regions, and largest in blue regions) for scattering of plane waves incident with direction $(1, 0)^T$ and $(0, 1)^T$, and ∂D is plotted over this for comparison. We see that that the smallest values of δ^α occur on ∂D. However, the problem of non-uniqueness for our approximation is illustrated in that some parts of ∂D are 'picked out' in the same detail as points not on the boundary, whilst some parts of ∂D are not identified at all.

In figures 8.6 and 8.7 we illustrate our total field reconstructions alongside the field as calculated using our numerical method for the direct problem, for comparison. Rather than α or β we give the relative error in solving (5.1). We see that some features of the field such as (especially symmetry) are present in the reconstructions, and that the range of values that the real part of the 'actual' and reconstructed field attains are similar.

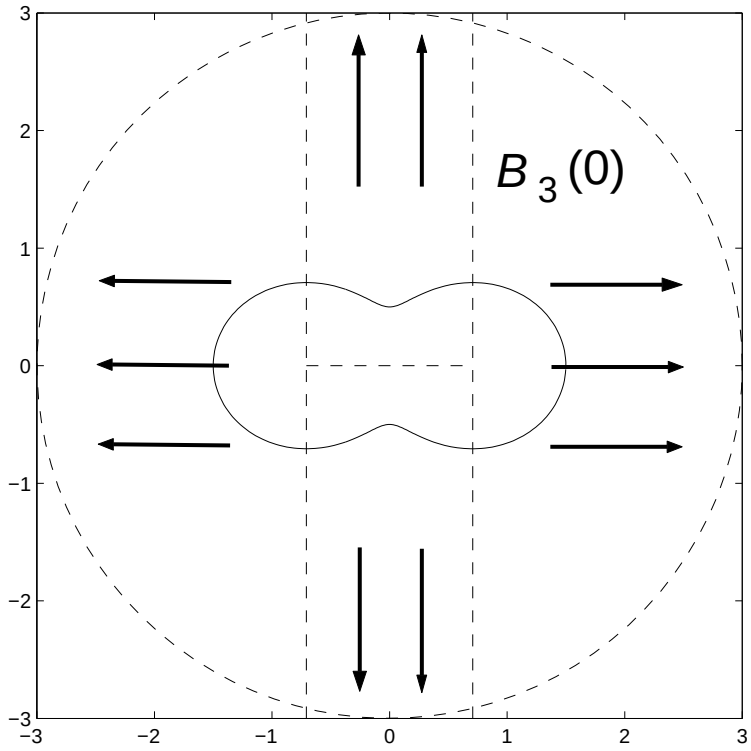

Figure 6.6: Cone directions

Chapter 7

Conclusions and Further Work

We have presented and implemented the method of R. Potthast for reconstructing the total field about a sound-soft scatterer, using a finite number of measurements of the corresponding far-field pattern, and shown that it is possible to use this method to locate the boundary of the scatterer. However, we must question the practicability of this method.

It is conceivable that we can bound the location of the scatterer, and so find some direction $\hat{\mathbf{t}}$ in which to direct our incident plane wave, and some point $\mathbf{x} \in \mathbb{R}^m \backslash \bar{D}$ at which to measure the total field. From this we subtract the known incident field at $\mathbf{x}$ to obtain the scattered field at $\mathbf{x}$. Then, it is simply a matter of using the asymptotic behaviour of all radiating solutions to the Helmholtz equation to obtain a $O(1/|\mathbf{x}|)$ approximation to the corresponding far-field pattern in direction $\hat{\mathbf{x}}$

$$u^\infty(\hat{\mathbf{x}}, \hat{\mathbf{t}}) = |\mathbf{x}|^{\frac{m-1}{2}} e^{-i\kappa|\mathbf{x}|} u^s(\mathbf{x}, \hat{\mathbf{t}}) + O(\frac{1}{|\mathbf{x}|})$$

and therefore the success of the method in practice depends very much on the distance between the scatterer and the observer (relative to the wavelength).

We have seen that in locating the boundary of our scatterer from the reconstructed field, we also identify points that are not on the boundary, owing to the error in the field reconstruction. Therefore, it is likely that any practical attempt to use the method for an unknown sound-soft object will have to employ image processing software, using the data from the scattering of plane waves with differing directions and wave numbers.

Of course, the main impediment to the method of Potthast is that the error bounds on the field reconstruction only hold at points on the exterior of the scatter, for a suitable exterior cone condition and domain of approximation. We have applied the method for a known ∂D, but of course in practical applications this information is not available, and so

it is unclear as to how we might apply the method in general. An algorithmic approach might be successful, where, starting with some initial conditions the exterior cone condition and cone directions for our rotated G_0 are successively improved upon. However, again this would most likely require some sort of image processing stage at each update.

It remains a problem as to how to verify the accuracy of our field reconstructions. We can visually verify that certain characteristics of the total field are present in the reconstructions (figures 8.6 and 8.7) and even see that the range of values of the reconstructed field is similar to that of the actual field. However, it is not clear as to how we might test for convergence of the reconstruction in any mathematical sense. Clearly the field at some points is reconstructed more accurately than at others, making it hard to quantify the success of the reconstruction overall, and any approach to this problem is likely to disregard the reconstruction of field characteristics in favour of field values.

Inverse scattering is a modern and relevant area of mathematical physics, with many areas of application, and so there is much scope for further work. It would be interesting for instance, to apply the method to three dimensional scattering, as the theory holds in either of $\mathbb{R}^2$ or $\mathbb{R}^3$.

One area to look at is alternative choices for the geometry of G_0. In [8] Potthast presents a method for field reconstruction where G_0 is a disc, while Luke [6] uses a subtle variation on our G_0, specifically

$$G_0 = B_{R_1}(-\epsilon\mathbf{i})\backslash\{\mathcal{C}_{-\epsilon\mathbf{i},\mathbf{i},\beta} \cup B_{R_2}(-\epsilon\mathbf{i})\}$$

for some $0 < R_2 < R_1$ (whereas we have used $R_2 = 0$).

Of practical importance is the problem of 'noise': that is, an error in measuring the far-field pattern due to the system not being closed (for instance in practice it is likely that there will be other sources of acoustic waves not accounted for in the model, especially in outdoor applications) or due to the accuracy of the equipment used to measure the field. For instance, let $w^s(\mathbf{z}, \hat{\mathbf{t}})$ be our approximation to $u^s(\mathbf{z}, \hat{\mathbf{t}})$, which we remind the reader is given by

$$w^s(\mathbf{z}, \hat{\mathbf{t}}) = \frac{1}{\gamma_m} \int_\Omega u^\infty(-\hat{\mathbf{d}}, \hat{\mathbf{t}}) g_{\mathbf{z}}(\hat{\mathbf{d}}) dS(\hat{\mathbf{d}})$$

and for $\rho \geq 0$ let $u^\infty_\rho(., \hat{\mathbf{t}})$ be the far-field pattern obtained from our erroneous measurements, such that

$$|u^\infty(., \hat{\mathbf{t}}) - u^\infty_\rho(., \hat{\mathbf{t}})| \leq \rho$$

Then for

$$w_\rho^s(\mathbf{z},\hat{\mathbf{t}}) = \frac{1}{\gamma_m}\int_\Omega u_\rho^\infty(-\hat{\mathbf{d}},\hat{\mathbf{t}})g_{\mathbf{z}}(\hat{\mathbf{d}})dS(\hat{\mathbf{d}})$$

we have by the triangle inequality

$$|u^s(.,\hat{\mathbf{t}}) - w_\rho^s(.,\hat{\mathbf{t}})| \leq |u^s(.,\hat{\mathbf{t}}) - w^s(.,\hat{\mathbf{t}})| + |w^s(.,\hat{\mathbf{t}}) - w_\rho^s(.,\hat{\mathbf{t}})|$$

In section 4.3 we showed that we could bound $|u^s(.,\hat{\mathbf{t}}) - w^s(.,\hat{\mathbf{t}})|$ through our choice of G_0. As for the second term on the right hand side, we note that (by the Cauchy - Schwarz inequality)

$$\begin{aligned}
|w^s(.,\hat{\mathbf{t}}) - w_\rho^s(.,\hat{\mathbf{t}})| &= |\frac{1}{\gamma_m}\int_\Omega \{u^\infty(-\hat{\mathbf{d}},\hat{\mathbf{t}}) - u_\rho^\infty(-\hat{\mathbf{d}},\hat{\mathbf{t}})\}g_{\mathbf{z}}(\hat{\mathbf{d}})dS(\hat{\mathbf{d}})| \\
&\leq \frac{1}{|\gamma_m|}\|u^\infty(-\hat{\mathbf{d}},\hat{\mathbf{t}}) - u_\rho^\infty(-\hat{\mathbf{d}},\hat{\mathbf{t}})\|_{L^2(\Omega)}\|g_{\mathbf{z}}\|_{L^2(\Omega)} \\
&\leq \frac{\rho}{|\gamma_m|}\|g_{\mathbf{z}}\|_{L^2(\Omega)}
\end{aligned}$$

Therefore, if $\|\vec{h}^\alpha\|_2$ grows unboundedly as $\alpha \to 0$ in our numerical solution to the inverse problem, then any error in our far-field pattern measurement is amplified.

Finally, parallel to the work in acoustic scattering there is the problem of inverse electromagnetic scattering (radar scattering). We model the electromagnetic wave by its complex vector fields **E** (the *electric field*) and **H** (the *magnetic field*), and the in [7] Potthast approaches the inverse scattering problem in the same way as for the acoustic case. However, though sharing much with acoustic inverse scattering, this area of research has its own problems. For instance, the theorem in electromagnetic scattering that is the analogue of theorem 9 is not as strong, and so implementing a successful algorithm for edge location is even more of a problem than for the acoustic case.

Chapter 8

Figures

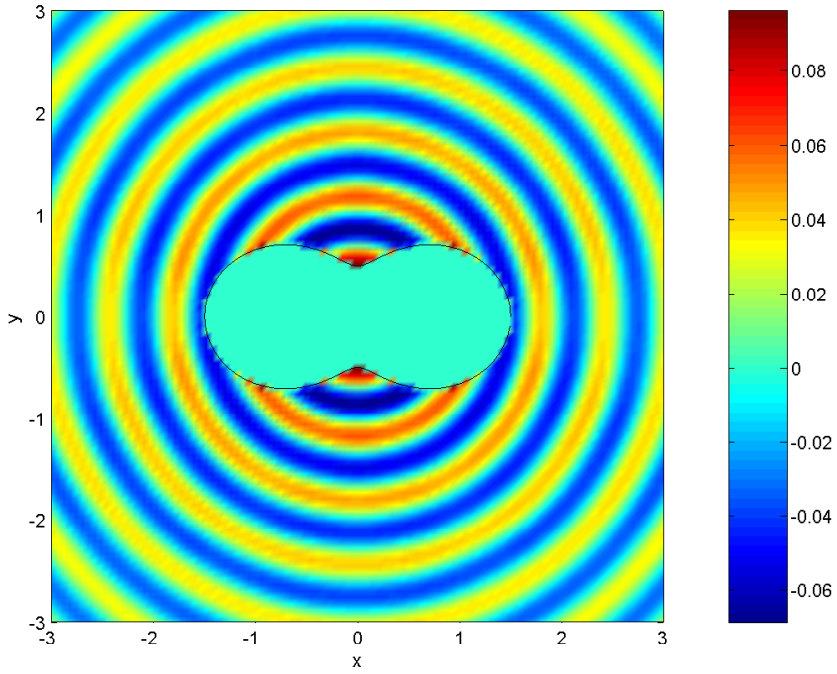

Figure 8.1: Real part of numerical solution to EADP for $g = \Phi(\mathbf{x}, \mathbf{0})$, $\kappa = 10$, on a 100×100 mesh, ∂D discretised by 100 points

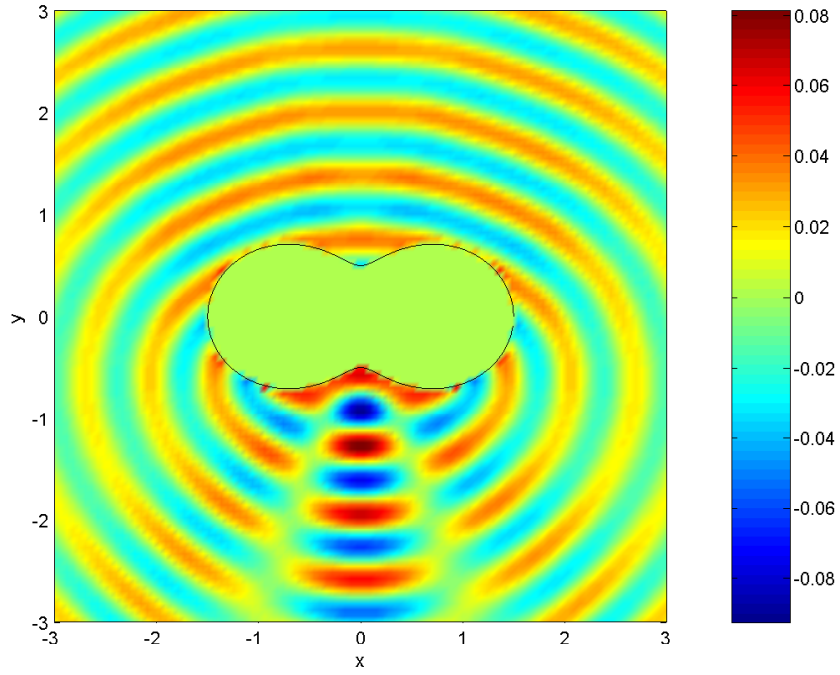

Figure 8.2: Real part of numerical solution to EADP for $g = -\Phi(\mathbf{x}, \mathbf{z})$ for $\mathbf{z} = (0, -2)^T$, $\kappa = 10$, on a 100×100 mesh, ∂D discretised by 100 points

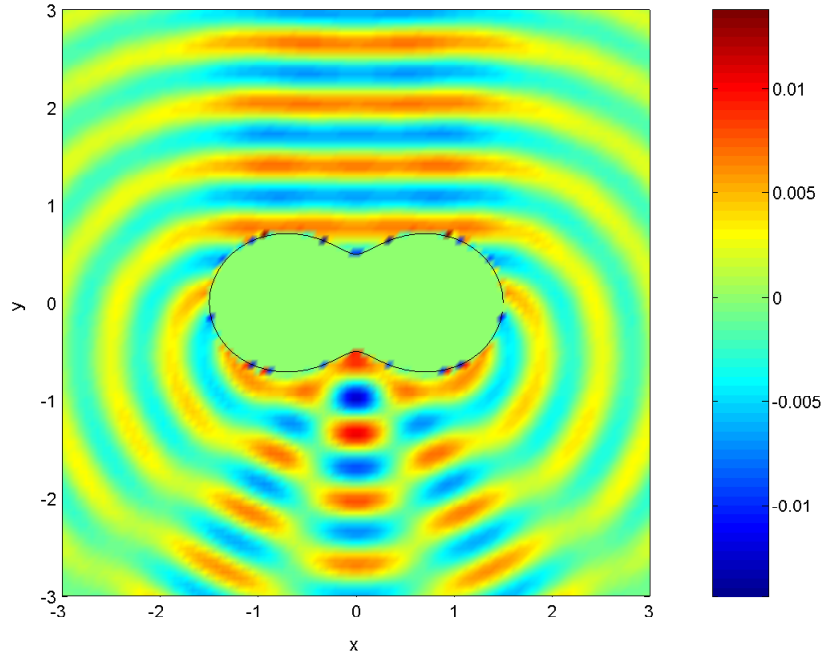

Figure 8.3: Real part of numerical solution to EADP for $g = -\Phi(\mathbf{x}, \mathbf{z})$ for $\mathbf{z} = (0, -100)^T$, $\kappa = 10$, on a 100×100 mesh, ∂D discretised by 100 points

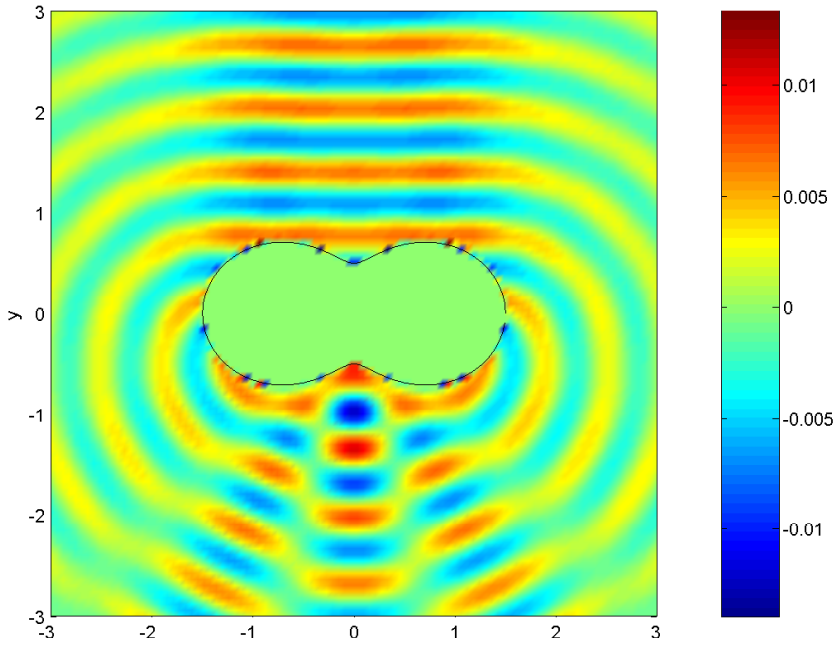

Figure 8.4: Real part of numerical solution to EADP for $g = -\Lambda(\mathbf{x}, \mathbf{z})$ for $\mathbf{z} = (0, -100)^T$, $\kappa = 10$, on a 100×100 mesh, ∂D discretised by 100 points

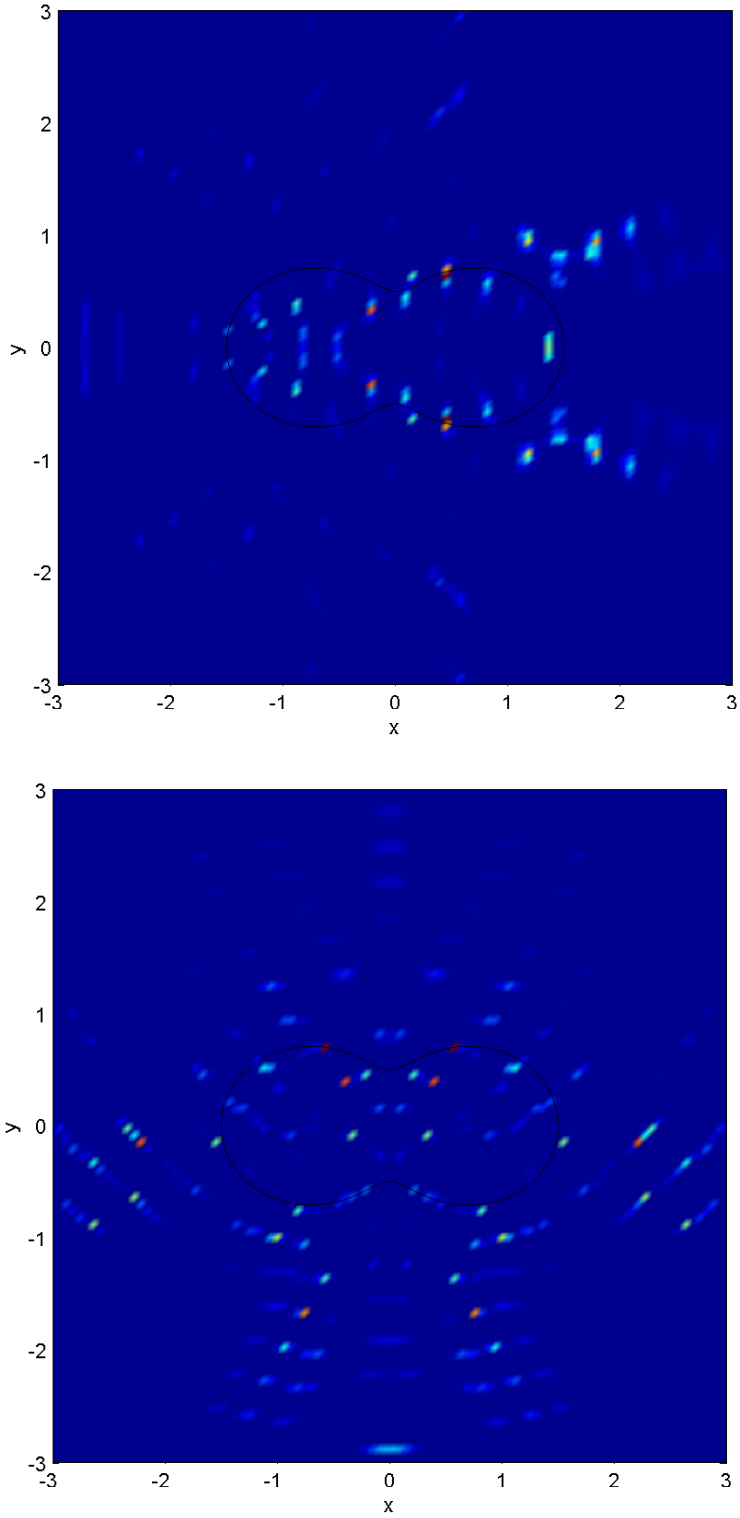

Figure 8.5: Edge location using an incident plane wave with direction $(1,0)^T$ (top) and direction $(0,1)^T$ (bottom), $\kappa = 10$, on a 100×100 mesh, ∂D discretised by 100 points, relative error in Tikhonov regularisation $= 0.3997$

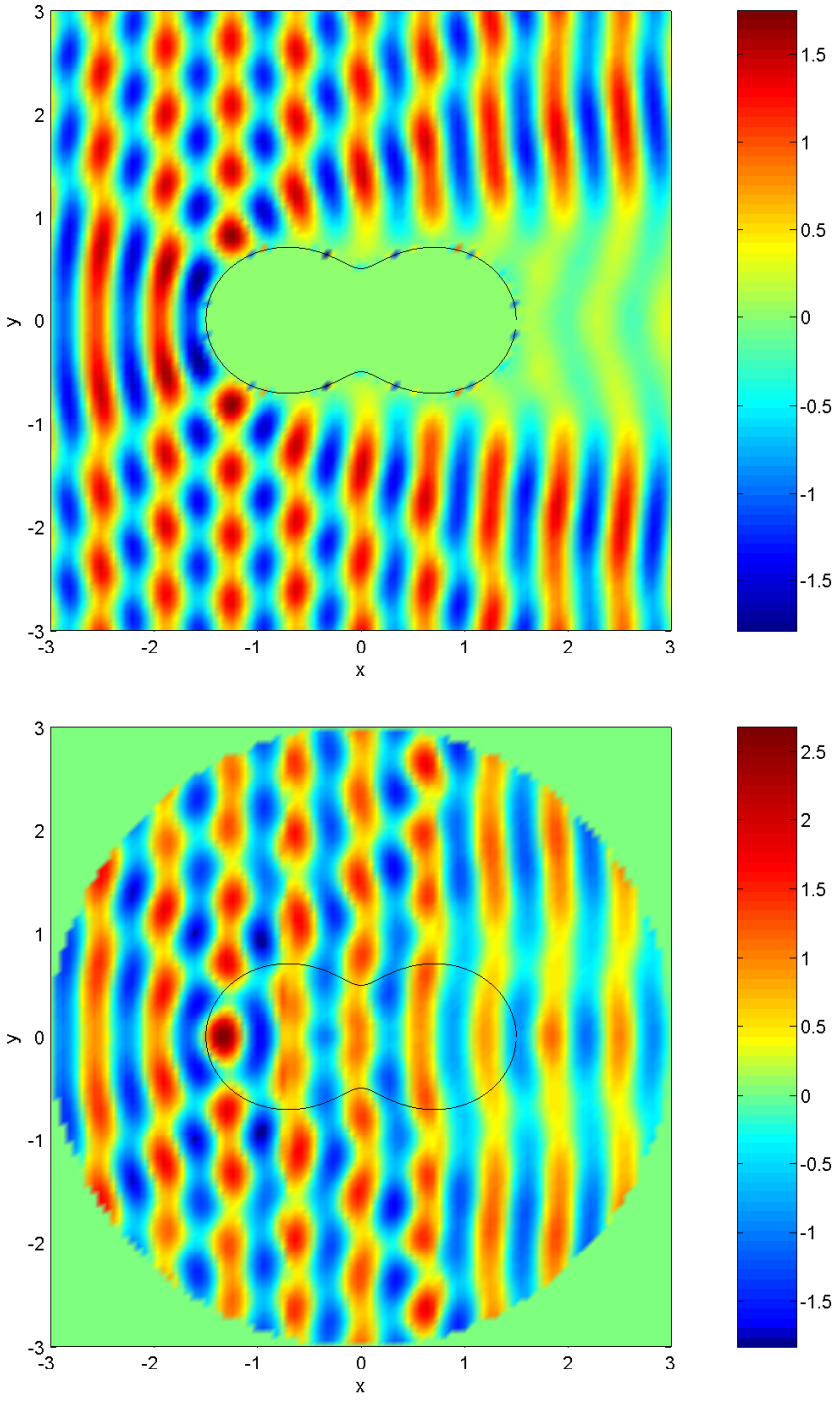

Figure 8.6: Real part of total field about $\bar{D}$ using direct method (top) and point source reconstruction (bottom) for scattering of an incident plane wave with direction $(1,0)^T$, $\kappa = 10$, on a 100×100 mesh. ∂D discretised by 100 points (top) and 200 points (bottom). Relative error in Tikhonov regularisation $= 0.3997$.

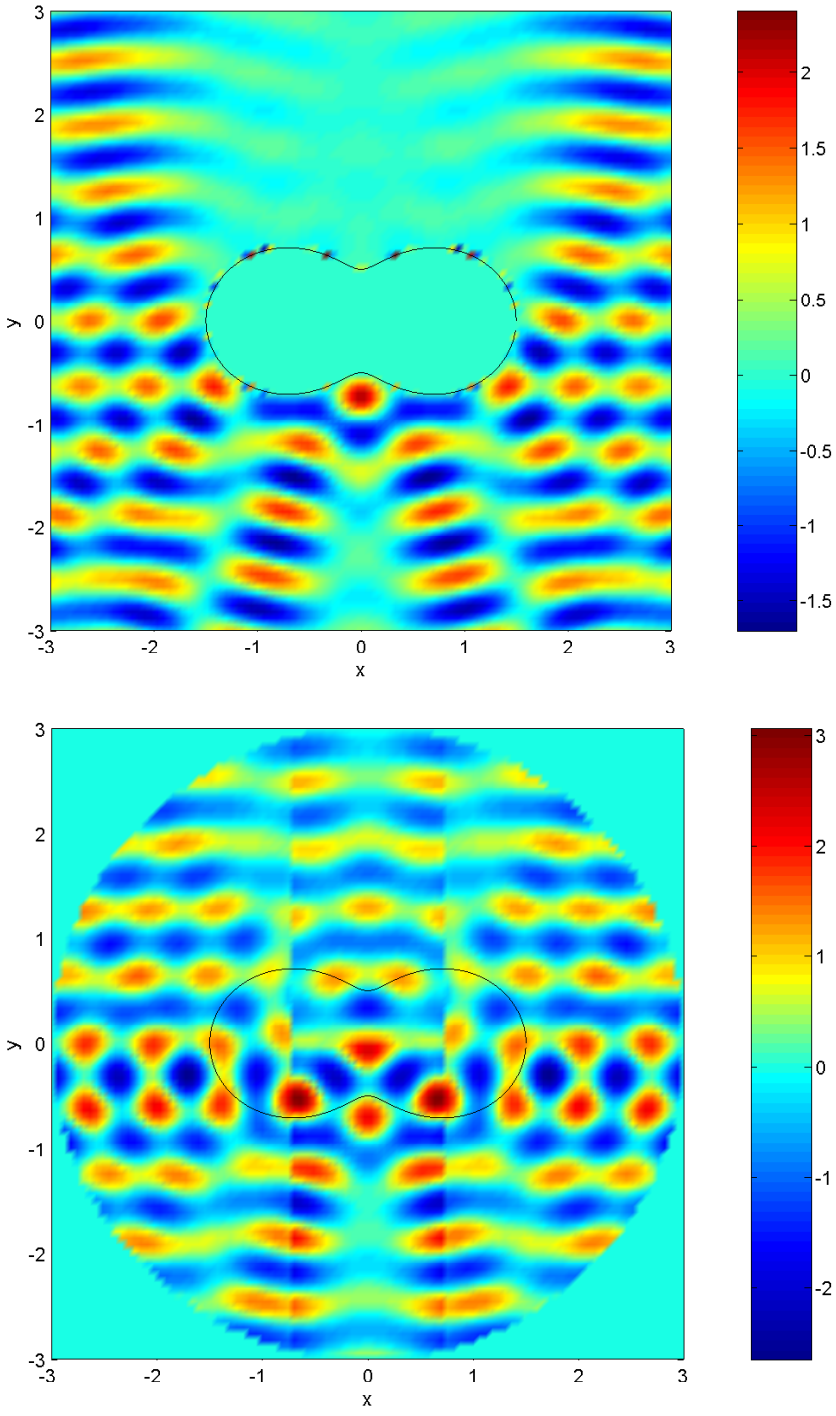

Figure 8.7: Real part of total field about $\bar{D}$ using direct method (top) and point source reconstruction (bottom) for scattering of an incident plane wave with direction $(0,1)^T$, $\kappa = 10$, on a 100×100 mesh. ∂D discretised by 100 points (top) and 200 points (bottom). Relative error in Tikhonov regularisation $= 0.3997$.

Bibliography

[1] W.W.Bell: *Special Functions for Scientists and Engineers*, D. Van Nostrand Company Ltd (1968)

[2] M.L.Boas: *Mathematical Methods in the Physical Sciences*, John Wiley & Sons, Inc. (1996)

[3] D. Colton & R Kress: *Inverse Acoustic and Electromagnetic Scattering Theory*, Springer (1998)

[4] D. Colton & R Kress: *Integral Equation Methods in Scattering Theory*, John Wiley & Sons, Inc. (1983)

[5] C. D. Lines: *Inverse Scattering by Unbounded Rough Surfaces*, PhD thesis, Brunel University, 2003

[6] R. Luke: *Multifequency inverse obstacle scattering: the point source method and generalized filtered backprojection*, Pacific Institute for the Mathematical Sciences preprint number PIMS-03-04

[7] R. Potthast: *A point source method for inverse acoustic and electromagnetic obstacle scattering problems*, IMA Journal of Applied Mathematics vol. 61, 119-140 (1998)

[8] R. Potthast: *The point source method for reconstructing an inclusion from boundary measurements in electrical impedance tomography and acoustic scattering*, Inverse Problems vol. 19, 1139-1157 (2003)

[9] R. Potthast: *Point Sources and Multipoles in Inverse Scattering Theory*, Chapman & Hall/CRC (2001)